MODELS FOR MAGNETIC RESONANCE OBSERVATION OF DIFFUSION IN CELLULAR ENVIRONMENTS

by

Muhammet Memiç

B.S., Physics, Boğaziçi University, 2012

Submitted to the Institute for Graduate Studies in
Science and Engineering in partial fulfillment of
the requirements for the degree of
Master of Science

Graduate Program in Physics

Boğaziçi University

2015

MODELS FOR MAGNETIC RESONANCE OBSERVATION OF DIFFUSION IN CELLULAR ENVIRONMENTS

APPROVED BY:

Assist. Prof. Evren Özarslan (Thesis Supervisor)	.....
Assoc. Prof. Mehmet Burçin Ünlü	.....
Prof. Pemra Doruker Turgut	.....

DATE OF APPROVAL: 10.08.2015

ACKNOWLEDGEMENTS

First, I would like to give my deep gratitude to Evren Özarslan for his immense efforts. This thesis is done with his patience, support, advices, guidence, valuable comments and suggestions.

I would also like to thank Cem Yolcu and Maryam Afzali for their contributions to my thesis. Last but not least, I would like to thank Spinoza lab members for their friendship.

ABSTRACT

MODELS FOR MAGNETIC RESONANCE OBSERVATION OF DIFFUSION IN CELLULAR ENVIRONMENTS

Diffusion tensor imaging (DTI) is a widely used way of mapping anatomical connectivity in the brain. However, it is based on two basic features that limit the validity of the model : (i) It is a Gaussian based model. However, studies show that the diffusion in tissue has a restrictive character. (ii) Multiple fiber directions are indistinguishable within a single voxel since Gaussian probability distribution gives only one directional maximum. This thesis consists of two parts. In the first part, a model alternative to DTI will be suggested to characterize diffusion anisotropy. Diffusion-attenuated MR signal for molecules under the influence of a parabolic potential will be discussed. Signal expression under such potential can be obtained by solving the modified Bloch-Torrey equation via multiple correlation function (MCF) framework with the addition of a potential term . Diffusion anisotropy is introduced by a stiffness tensor rather than a diffusion tensor. In the second part, an alternative diffusion sensitization mechanism is provided by employing rotating field gradiens (RFGs) which leads to a way of measuring the diffusion orientation distribution function (dODF) directly. Then, RFG results for both free and restricted diffusion model (proposed model in the first part) will be compared with results obtained by traditional pulsed field gradient (PFG) based models: Q-ball imaging (QBI) and its extension to constant solid angles (CSA).

ÖZET

HÜCRESEL ORTAMLARDAKİ YAYINIMIN MANYETİK REZONANS GÖZLEMİ İÇİN MODELLER

Yayınım tensör görüntüleme (DTI) yöntemi beyindeki anatomik bağlanırlığı haritalandırmada yaygınca kullanılan bir yöntemdir. Fakat modelin geçerliliğini kısıtlayan iki temel özellik vardır : (i) Yayınım tensör görüntüleme Gauss tipi dağılım temelli bir modeldir. Ama çalışmalar dokudaki yayınımın kısıtlayıcı özellikte olduklarını göstermiştir. (ii) Tek bir vokseldeki çoklu fiber yönleri Gauss tipi dağılımın sadece bir yönsel maksimum vermesinden dolayı ayırt edilemez. Tez iki kısımdan oluşmaktadır. İlk kısımda yayınımın yöne bağımlılığını betimlemek için, yayınım tensör görüntüleme yöntemine alternatif bir model tavsiye edilmiştir. Parabolik potensiyelin etkisi altındaki moleküllerin yayınımı azalmış manyetik rezonans sinyali tartışılmıştır. Bu potensiyel altındaki sinyal ifadesi potensiyel teriminin eklenmesiyle değişmiş Bloch-Torrey denkleminin çoklu korelasyon fonksiyonu (MCF) yardımıyla elde edilmiştir. Yayınımın yöne bağımlılığı yayınım tensöründen ziyade gerginlik tensörüyle tanımlanmıştır. İkinci kısımda yayınıma duyarlılık mekanizması dönen alan gradyanları (RFGs) uygulanarak sağlanacaktır. Dönen alan gradyanı uygulamak yayınım yönsel dağılım fonksiyonunu doğrudan ölçmenin bir yoludur. Bu sekans için serbest ve kısıtlanmış yayınım sonuçları, geleneksel darbeli alan gradyanı temelli olan modellerden elde edilmiş sonuçlar ile karşılaştırılacaktır.

TABLE OF CONTENTS

LIST OF FIGURES

LIST OF SYMBOLS

B_0	Main magnetic field
D_0	Diffusion coefficient
G	Magnitude of a gradient
k	Boltzmann constant
$\mathbf{q}$	Gradient wave vector
t_m	Mixing time
γ	Gyromagnetic ratio
Δ	Diffusion time
δ	Duration of applied gradient
θ	Angle between applied gradient and the z direction
ω	Larmor frequency
$\mathbf{\Omega}$	Stiffness tensor

LIST OF ACRONYMS/ABBREVIATIONS

ADC	Apparent Diffusion Coefficient
CSA	Compartment Shape Anisotropy
dODF	Diffusion Orientation Distribution Function
DTI	Diffusion Tensor Imaging
EA	Ensembe Anisotropy
MCF	Multiple Correlation Function
MP	Multiple Propagator
NMR	Nuclear Magnetic Resonance
PDF	Probability Distribution Function
PFG	Pulsed Field Gradient
QBI	Q-Ball Imaging
QSI	Q-Space Imaging
RF	Radio Frequency
TE	Echo Time
μA	Microscopic Anisotropy

1. INTRODUCTION

Diffusion weighted magnetic resonance imaging (dMRI) has been a widely used technique that allows to map the anatomical connections between different regions of the brain. It reflects white matter fiber structure and highly valueble information about brain connectivity. Different imaging techniques have been suggested to explore the white matter connectivity in the brain such as diffusion tensor imaging (DTI), Q-space imaging (QSI). Diffusion process of water molecule is investigated since cells mostly contain water. Path of a water molecule is determined by the geometry of structure. To probe the underlying neurol structure, sensitization mechanisms are introduced for mobility of water in the brain.

Diffusion of spin-bearing particles is affected by the structure of porous materials, colloidal systems and biological tissue. Thus diffusion measurement is a very important source of information in diagnosing numerous diseases and treatments [6–14]. It is required that movement of such particles should be modelled in tissue. DTI is the first suggested model for mapping the tissue of architecture in vivo noninvasively [15, 16]. It is based on Gaussian diffusion within each voxel. DTI will be discussed in detail in a subsequent section. However, it is known that diffusion process is restricted and very complex [17–21]. The complexity due to the microstructure of tissue must be revealed by models.

Diffusion process in tissue contains a lot of information since diffusion rates of particles are not the same in everywhere. It highly depends on celluler environments. Cells are extremely crowded places that contain many different structures such as macromolecules, organelles, fibers and membranes. Such obstacles inside the cell affect the diffusion process because particle's movement is restricted by some bounderies. Thus, a change in the diffusion process reveals microstructure of the tissue. Briefly due to the complexity in the tissue, diffusion is not free.

1.1. Diffusion in MR

Diffusion is a process that is a result of random collisions between molecules in a fluid. This phenomenon is known as Brownian motion. Einstein showed that such a random motion is driven by thermal energy of the particles [22] . If we define displacement probability $P(x,t)$ where x is relative position of a particle at the time t, diffusion can be described by

$$\frac{\partial P(x,t)}{\partial t} = D_0 \nabla^2 P(x,t) \tag{1.1}$$

where the D_0 is the diffusion constant. In the assumption that particles are initially at the origin represented by a delta function $\delta(x)$ and $P(x,t)$ aproaches to zero when x goes to $\pm\infty$, solution of Equation 1.1. with the associated initial and boundary conditions is

$$P(x,t) = \frac{1}{\sqrt{4\pi D_0 t}} \exp\left(-\frac{x^2}{4D_0 t}\right) \tag{1.2}$$

When the molecules are diffusing freely without striking any obstacles, displacement probability distribution $P(x,t)$ is Gaussian. Probability of finding a particle in the initial location will decrease after a period of time due to diffusion as plotted in Figure 1.1. So mean squared displacement for free diffusion is given by

$$\left\langle x^2 \right\rangle = \int P(x,t) x^2 dt \tag{1.3}$$

Calculation of above integral yields the Einstein relation which can also be interpreted as the variance of the positions

$$\left\langle x^2 \right\rangle = 2D_0 t \tag{1.4}$$

This relation is very important because mean squared displacement for a time interval is a measurable quantity that enables us to determine the diffusion coefficient. Thus,

Nuclear magnetic resonance (NMR) imaging is a technique that allows to measure the mean square displacement of the spins by applying pulse sequences in order to extract the diffusion coefficient. Now, I will give some basics of how pulse sequences produce signal from a porous media.

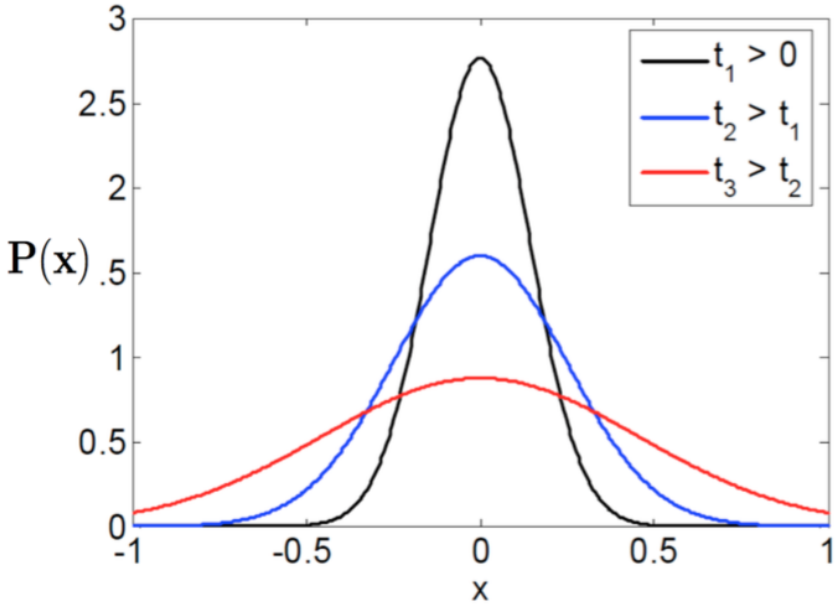

Figure 1.1. Normal distributions of particles for different time periods are illustrated in this figure.

1.2. Sensitization Mechanism

In the light of the Einstein relation, how diffusion coefficient could be estimated by using NMR had been demonstrated. Erwin Hahn can be known as a first people who are interested in diffusive NMR [23]. In 1950, he applied spin echo sequence which contains two successive radio frequencies (RF) 90° and 180° separated by a time $TE/2$ as demonstrated in Figure 1.2. The 90° RF pulse turns magnetization into the transverse plane and then starts to dephasing. After applying refocusing 180° RF pulse, stationary spins are completely refocused and an echo signal is observed at time TE. In reality, however, there is always diffusion.

Due to the inhomogeneity in the magnetic field, signal obtained from diffusing spins are not completely refocused at time TE. Such a situation causes a drop in the signal. That is why the spin echo sequence is a touchstone for measuring diffusion.

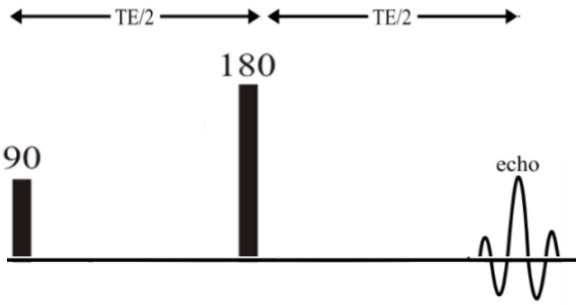

Figure 1.2. Hahn spin echo sequence consists of 90° RF pulse followed by 180° separated by the time $TE/2$ and spin echo occurs at the time TE.

In 1954, Carr and Purcell gave the extended version of spin echo sequence [24]. They applied 180° RF pulse repeatedly for minimizing the diffusion effect and generated multiple spin echoes. In 1956, Torrey generalized the Bloch equations which represent the equation of motion for nuclear magnetization. He included a term to account for transfer of magnetization transfer via diffusion [25]. In 1967, Stejskal and Tanner modified the Hahn spin echo sequence by including two diffusion weighting gradients around 180° RF pulse [26] instead of steady gradient as shown in Figure 1.3. They solved Bloch-Torrey equation for two symmetric rectangular pulsed gradients, which give rise to better sensitivity to diffusion in comparison to Hahn spin echo sequence. Let's start with a qualitative description of diffusion on NMR signal from a physical point of view.

When spins are exposed to a magnetic field, magnetic moment of spins will align with the applied field which exerts a torque on the spins and they start to precess about the magnetic field. This phenomenon is called Larmor precession. Angular frequency $\omega = \frac{d\phi}{dt}$ of this precession is given by

$$\omega = \gamma B_0 \tag{1.5}$$

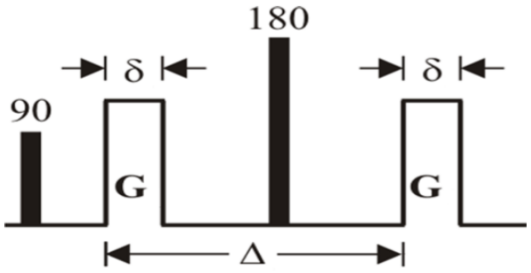

Figure 1.3. Addition of two diffusion sensitizing gradient with a duration δ to a spin-echo sequence is depicted.

where B_0 is the applied magnetic field and γ is the gyromagnetic ratio.

In addition to the main magnetic field B_0, gradients G are applied momentarily,which changes B_0 spatially. When there is a spatially dependent magnetic field gradient G, spin's precession rate will become position dependent. Some spins will precess faster than others due to time dependent inhomogeneous magnetic field while when all the spins experience the same magnetic field B_0, their precession frequencies will be the same regardless of position. Using the advantage of spatial dependence of Larmor frequency, we can label the position of spins using Stejskal-Tanner pulse (s-PFG) by means of changes in the Larmor frequency. Aplication of the first gradient G with a duration of δ results in an accumulated phase which is given by

$$\phi_1(t) = \gamma \int_0^t G(t')z(t')dt' = \gamma G_z \delta z_1 \tag{1.6}$$

assuming that gradient is applied in the direction of z so we are able to measure the diffusion in that direction and z_1 is the initial position of the spin. The second gradient with the same magnitude is applied after waiting for a diffusion time Δ and corresponding phase shift is given by

$$\phi_2(t) = \gamma G_z \delta z_2 \tag{1.7}$$

where z_2 is the new position of the spin after aplication of the second gradient. So net phase shift is

$$\phi_1 - \phi_2 = \gamma G \delta (z_1 - z_2) \tag{1.8}$$

In the absence of diffusion, location of the spin does not change ($i.e. z_1 = z_2$). Net phase shift will be zero and signal is not attenuated. In case of diffusion, however, some spins move to a different location, which second gradient encodes at different places. Therefore, they are partially refocused. That causes reduction in the signal.

1.3. Relation Between Signal Attenuation And Diffusion Propagator

Signal can be obtained from an ensemble of spins diffusing in a confining domain. So macroscopic signal E represents averaging phase over this ensemble

$$E = \left\langle \exp(-i\gamma \int_0^{TE} dt \mathbf{G}(t) \cdot \mathbf{r}(t)) \right\rangle \tag{1.9}$$

where the signal E is obtained by applying magnetic field gradient $\mathbf{G}(t)$ of duration TE noting that E is a normalized quantity that takes the value of 1 when $\mathbf{G}(t)$ is equal to 0. Signal expression can be written in terms of two new quantities: $P_\Delta(r_1, r_2)$ and $\rho(r_1)$

$$E = \int \rho(r_1) \int P_\Delta(r_1, r_2) e^{-iq(r_2 - r_1)} dr_1 dr_2 \tag{1.10}$$

$P_\Delta(r_1, r_2)$ is the probability of finding a spin at position r_2 at the time Δ, the time between two gradients, such that it is initially located at r_1 and $\rho(r_1)$ is the spin density at the moment when the first pulse is applied. Note that $q = (2\pi)^{-1}\gamma\delta G$. In the limit that the diffusion time Δ goes to infinity, $P_\Delta(r_1, r_2)$ approaches to $\rho(r_1)$ since a spin can be found in any position with the same probability. If we assign a new variable

$R = r_2 - r_1$, Equation 1.10 becomes the following:

$$E = \int dR\overline{P}_{\Delta}(R)e^{-iqR} \tag{1.11}$$

where $\overline{P}_{\Delta}(R)$ is the average propagator which is given by

$$\overline{P}_{\Delta}(R) = \int \rho(r_1)\overline{P}_{\Delta}(r_1 + R)dr_1 \tag{1.12}$$

Signal intensity will be the Fourier transform of the $\overline{P}_{\Delta}(R)$. If one takes the inverse Fourier transform of Equation 1.11, the average propagator can be obtained. This is known as $q-$space formalism [27]. The average propagator $\overline{P}_{\Delta}(R)$ can be obtained exactly when the pulses with infinitesimally short durations are applied. Since when the rectangular pulses are applied, diffusion takes place during the pulses and such a situation affects the NMR measurements. Technical limitations do not allow to apply the pulsed field gradient with minimum duration. However, the condition of δ being much smaller than Δ ensures a good approximation for finite value of δ. That is why narrow pulse condition is required for minimizing the effect of diffusion during the finite gradient pulses.

1.3.1. Signal Expression For Isotropic, Unrestricted Diffusion

When the diffusion is unrestricted and isotropic, it means that particles are moving freely. The propagator is a Gaussian function and it is represented in Equation 1.2. Then the signal attenuation expression can be obtained after the substitution of the propagator into the Fourier relation in Equation 1.10.

$$E(q, \Delta) = e^{-4\pi q^2 D_0 \Delta} \tag{1.13}$$

The linear relationship between mean-squared displacement and diffusion time (See: Equation 1.4) is caused by free Gaussian. Then the MR signal attenuation is monoexponential. However, when the particle's movement are limited by boundaries, such a

relationship will no longer become valid. For example molecules in white matter diffuses along the axons because of the fact that orientation of the myelin sheets restrict the motion. In case of short diffusion time Δ, molecules exhibit Gaussian distribution since they may not have a chance to reach the boundary. On the other hand, if the diffusion time Δ is so long that molecules are able to feel the effect of restriction or to give opportunity to move between intracellular and extracellular compartments, probability distribution does not remain Gaussian and non-monoexponential signal decay is observed [28, 29]. Deviation from Gaussianity results in a decrease in the measured diffusion coefficient. Dependence on Δ implies that diffusion coefficient is a function of Δ.

1.3.2. Signal Expression For Anisotropic or Restricted Diffusion

Anisotropic or restricted diffusion was investigated by Stejskal [30] using single-PFG acquisitions. Two different examples of systems has been suggested in his paper to show the evidence of the restricted diffusion. First example giving restrictive behaviour is that diffusion occurs in a parallel layers with a finite thickness (Laminar flow). The other example that we are mainly interested in is that molecules are diffusing in a isotropic medium with scalar diffusion coefficient D_0 under a harmonic potential that results in a force.

$$\frac{\partial P}{\partial t} = D_0 \nabla^2 P + D_0 \beta f \nabla \cdot (\mathbf{r} P) \tag{1.14}$$

where f is the spring constant and $\beta = (k_B T)^{-1}$. Solution of such a partial differential equation is given by [31]

$$P_t(\mathbf{r}_0, \mathbf{r}) = \left[\frac{2\pi D_0 (1 - e^{-2\Omega t})}{\Omega}\right]^{-3/2} \exp\left[-\frac{\Omega(\mathbf{r} - \mathbf{r}_0 e^{-\Omega t})^2}{2D_0(1 - e^{-2\Omega t})}\right] \tag{1.15}$$

where $P_t(\mathbf{r}_0, \mathbf{r})$ is the conditional probability that a particle can be found at location $\mathbf{r}$ a time t later provided that it is initially located at $\mathbf{r}$ and $\Omega = \beta f D_0$. In the long time

limit, $P_t(\mathbf{r}_0, \mathbf{r})$ reaches the equilibrium density $\rho(\mathbf{r}_0)$

$$\rho_0 = \left[\frac{2\pi D_0}{\Omega}\right]^{-3/2} \exp\left(-\Omega \mathbf{r}_0^2 / 2D_0\right) \tag{1.16}$$

If one substitutes $P_t(\mathbf{r}_0, \mathbf{r})$ and $\rho(\mathbf{r}_0)$ into Equation 1.10, signal expression can be written as

$$E = \exp\left(-4\pi q^2 D_0 (1 - e^{-\Omega\Delta})/\Omega\right) \tag{1.17}$$

It can be seen that D_0 acquired by free diffusion expression in Equation 1.12. is replaced by the effective diffusion coefficient D_{eff}=$D_0(1 - e^{-\Omega\Delta})/\Omega$ which demonstrates MR signal attenuation depends on Δ. For Δ being close to zero, D_{eff} approaches to D_0. It exhibits free diffusion behavior. For $\Delta \to \infty$, $P_t(\mathbf{r}_0, \mathbf{r})$ approaches to $\rho(\mathbf{r}_0)$ as indicated above. So signal expression becomes $|S(\mathbf{q})|^2$ where $S(\mathbf{q})$ is the Fourier transform of the equilibrium density $\rho(\mathbf{r}_0)$ in the light of Equation 1.10.

1.4. Bloch-Torrey Equation

Another method for calculating the NMR signal under any time-dependent gradient waveform was made by Torrey [25]. Torrey modified the Bloch equations [32] by including a new term that represents the effect of diffusion. This equation is known as Bloch-Torrey equation as follows:

$$\frac{\partial \mathbf{M}}{\partial t} = \gamma(\mathbf{M} \times \mathbf{B}_0) + \begin{pmatrix} -\frac{M_x}{T_2} \\ -\frac{M_y}{T_2} \\ \frac{M_0 - M_z}{T_1} \end{pmatrix} + D\nabla^2 \mathbf{M} \tag{1.18}$$

where $\mathbf{M}$ is the magnetization density and diffusion constant D is a scalar assuming that diffusion rate is equall in all directions (isotropic). Above equation without the last term is the Bloch equation. Last term represents transport of magnetization. Signal

attenuation expression in the presence of gradient can be found

$$E = \frac{S}{S_0} = e^{-bD} \tag{1.19}$$

where S_0 is the maximum signal or signal accumulated without gradients S is the observed signal intensity when gradients are applied. Then, b is given by

$$b = \gamma^2 \int_0^{TE} \left(\int_0^t G(t')dt' \right)^2 dt \tag{1.20}$$

The parameter b is commonly used in diffusion-weighted imaging. It is experimentally controlable parameter. $b-value$ depends on both magnitude of gradient and diffusion time. Measuring the signal for different b values enables the diffusion coefficient D. Solving Equation 1.20 for Stejskal-Tanner pulse (See: Figure 1.3), b can be found with the correction term $\delta/3$ in comparison with signal predicted by q-space analysis.

$$b = \gamma^2 G^2 \delta^2 (\Delta - \frac{\delta}{3}) \tag{1.21}$$

Equation 1.19 can be rewritten as

$$S = S_0 \exp\left[\gamma^2 G^2 \delta^2 (\Delta - \frac{\delta}{3}) D\right] \tag{1.22}$$

This equation is valid for particles that has a Gaussian probability distribution. However diffusion in tissue is influenced by so many factors such as tissue architecture, membranes and organelles. Such factors that affect the free diffusion lead to modify the probability distribution and that causes reduction in the measured diffusion coefficient in the tissue. In case of free diffusion, particles are not restricted by any boundaries (Gaussian) and diffusion coefficient is the same for all directions. If you look at Equation 1.4. (Einstein relation) , there is a correlation between mean-squared displacement and diffusion time. For unrestricted diffusion, mean-squared displacement increases linearly with the diffusion time and diffusion coefficient does not change. Figure 1.4 shows the difference between free and restricted diffusion. Here, selecting the

diffusion time is very important since at small diffusion times particles move but not encounter the boundary of the compartment while particles experience the restriction as the diffusion time is adequately long. After sufficiently long times root mean-squared displacement reaches maximum value for restricted diffusion, which represents the com-

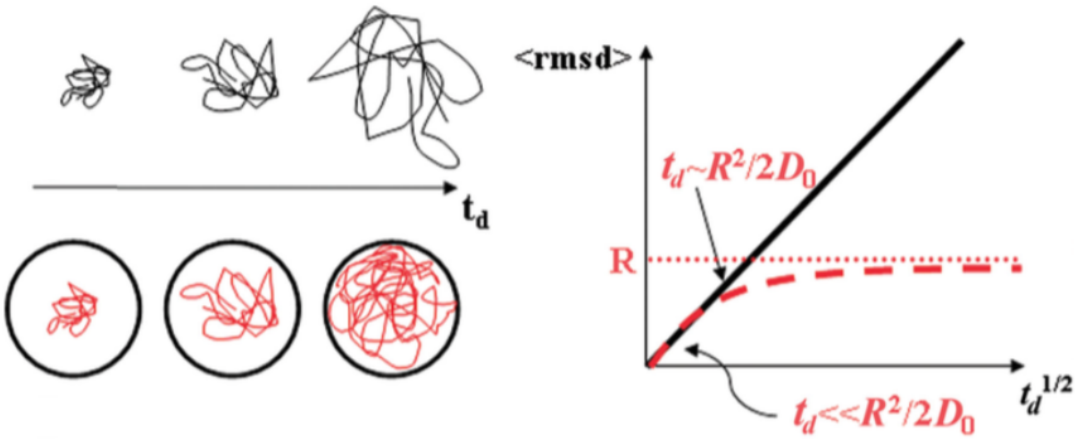

Figure 1.4. Left panel illustrates how the pathway of a particle for different diffusion periods is changed for both free and restricted diffusion. In right panel, root mean-square displacement is plotted against diffusion time. Black and red (dotted) lines show free and restricted diffusion respectively. R is related to the compartment size [1].

partment size. Probability distribution or diffusion is no longer Gaussian in case of restricted diffusion. So diffusion coefficient reflects free or restricted diffusion. To characterize these different mechanisms, apparent diffusion coefficient (ADC) is introduced. In restricted diffusion ADC is less than the diffusion coefficient in free diffusion.

1.5. Diffusion Tensor Imaging

When particles move freely without experiencing any obstacles, the same signal will be obtained from the sample. This is refered to as isotropic diffusion (e.g. gray matter). Diffusion rate is equal in all direction. Signal does not depend on orientation of the applied gradient. A single measurement in any direction is enough to extract

diffusion constant. On the other hand, Diffusion can depend on the orientation of the tissue or fibers. Tissue structure is a distinctive mark for diffusion. In cylindrical structures such as white matter fibers (See: Figure 1.5), molecules can move freely along the axons while molecules are restricted perpendicular to the fiber direction. In the axial direction, diffusion is faster relatively and there is a large diffusion coefficient whereas in all other directions, diffusion is slower and diffusion coefficient becomes

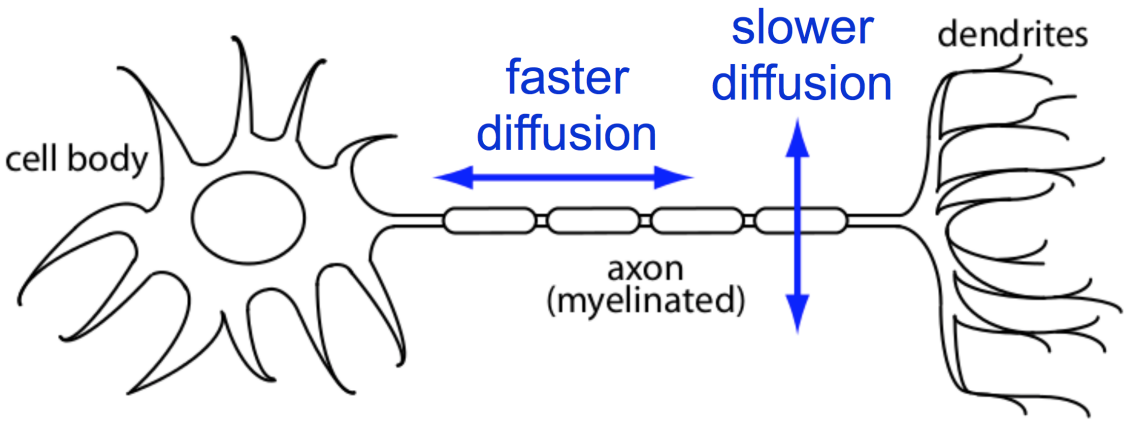

Figure 1.5. Representation of white matter fiber comprising diffusion anisotropy.

smaller. This is refered to as anisotropic diffusion. Obtained signal changes with respect to the measurement direction. Thus, no single quantity is attributed to characterize diffusivity. More developed model is required to account for anisotropic Gaussian diffusion. Concepts of isotropy, anisotropy, free and restricted diffusion are summerized in Figure 1.6.

Diffusion tensor imaging (DTI) is a magnetic resonance imaging technique that describes diffusion as a tensor . The tensor is a 3x3 symmetric matrix that consist of six elements and can be calculated in 3D space. It is usually represented as a ellipsoid (See: Figure 1.6). Measured signal S_i along the direction $\hat{r}_i$ can be written as

$$S_i = S_0 \exp(-b\hat{\mathbf{r}}_i{}^T \mathbf{D} \hat{\mathbf{r}}_i) \tag{1.23}$$

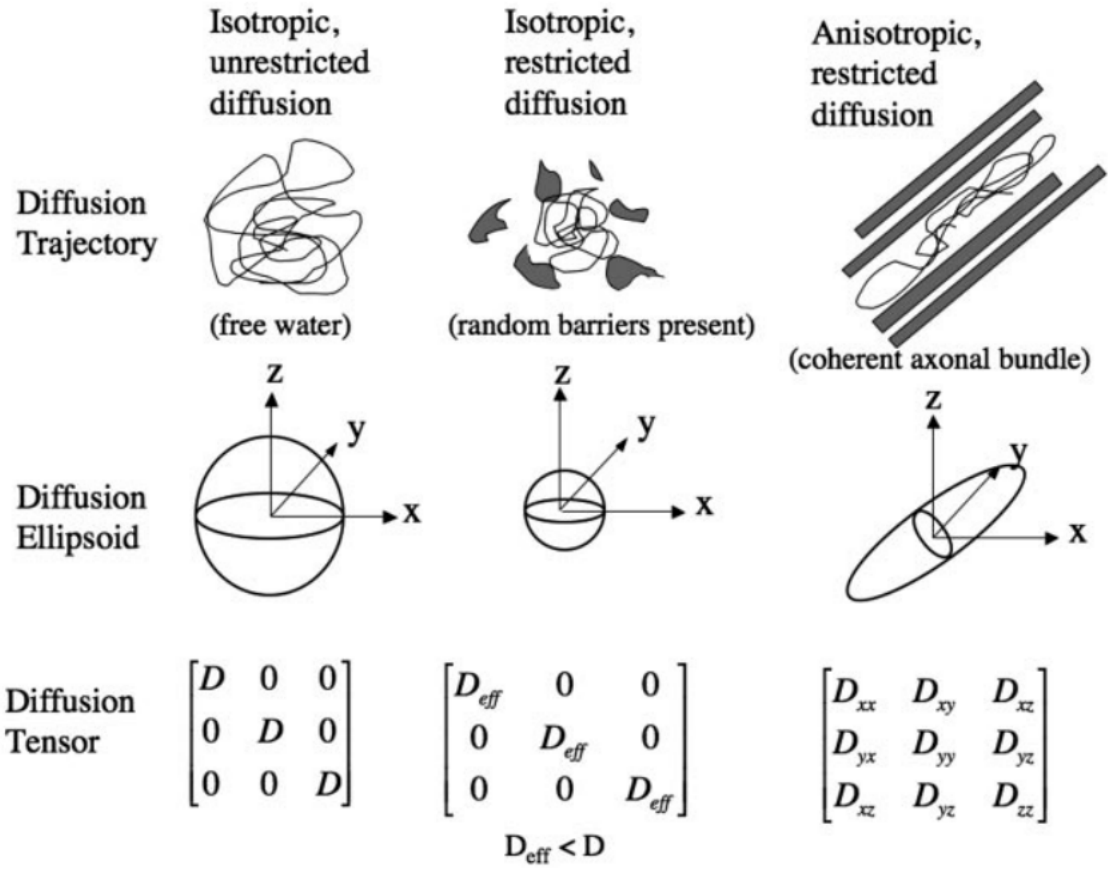

Figure 1.6. Different kinds of diffusion ellipsoids associated with their tensors are specifically demonstrated in Figure [2].

where S_0 is the signal when there is no applied gradient and b is the b-value for gradient G_i in the direction of $\hat{r_i}$ as indicated in Equation 1.14. 3x3 diffusion tensor is given by

$$\mathbf{D} = \begin{pmatrix} D_{xx} & D_{xy} & D_{xz} \\ D_{yx} & D_{yy} & D_{yz} \\ D_{zx} & D_{zy} & D_{zz} \end{pmatrix} \tag{1.24}$$

Since the diffusion tensor is symmetric (i.e. $D_{xy} = D_{yx}$), six different gradient directions are needed to determine the unknown elements of the matrix. These ADCs are obtained in the laboratory reference of frame for each voxel. However, ADCs in the local coordinate system for each voxel are required in order to determine the fiber direction. Here rotation matrices $\mathbf{R}$ are introduced for transforming a vector in the laboratory reference of frame to the principal axis frame. Thus, the measured tensor $\mathbf{D}$ must be diagonalized by spectral decomposition:

$$\mathbf{D} = \mathbf{R}^T \mathbf{D}_{local} \mathbf{R} \tag{1.25}$$

It also can be written in open form

$$\mathbf{D} = [\mathbf{e}_1|\mathbf{e}_2|\mathbf{e}_3]^T \begin{pmatrix} \lambda_1 & 0 & 0 \\ 0 & \lambda_2 & 0 \\ 0 & 0 & \lambda_3 \end{pmatrix} [\mathbf{e}_1|\mathbf{e}_2|\mathbf{e}_3] \tag{1.26}$$

where the eigenvectors $\mathbf{e}_1$, $\mathbf{e}_2$ and $\mathbf{e}_3$ are the orientation of the fibers that represent the maximum diffusivity along $\mathbf{e}_1$, $\mathbf{e}_2$ and $\mathbf{e}_3$, the eigenvalues λ_1, λ_2 and λ_3 reflect ADCs in the principal axis frame which is represented as the eigenvectors $\mathbf{e}_1$, $\mathbf{e}_2$, $\mathbf{e}_3$. Principal directions can be determined by the eigenvector where the maximum diffusion takes place. In case of isotropic diffusion, all the eigenvalues λ_1, λ_2 and λ_3 are equal and shape of ellipsoid reduces to sphere. On the other hand, if one of the eigenvalues is much larger than the others, diffusion is said to be anisotropic and represented as an ellipsoid (See: Figure 1.7). Principal direction provides information about the direction of the fiber orientation. So fiber orientation can be easily acquired by DTI. Different

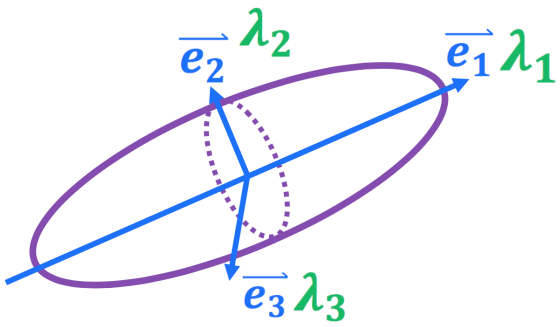

Figure 1.7. Eigenvectors and corresponding eigenvalues are represented as diffusion ellipsoid.

parts of the brain are connected via s-PFG acquisitions using anisotropy in the signal. The echo amplitude predicted by Stejskal-Tanner pulse (See: Equation 1.23) can be written as

$$E(\mathbf{b}) = \exp(-b[\hat{r_x}^2 D_{xx} + 2\hat{r_x}\hat{r_y}D_{xy} + 2\hat{r_x}\hat{r_z}D_{xz} + 2\hat{r_y}\hat{r_z}D_{yz} + \hat{r_y}^2 D_{yy} + \hat{r_z}^2 D_{zz}]) \quad (1.27)$$

For the sake of simplicity, we can describe gradients as a matrix so called b-matrix:

$$\mathbf{b} = b \begin{pmatrix} \hat{r_x} \\ \hat{r_y} \\ \hat{r_z} \end{pmatrix} \begin{pmatrix} \hat{r_x} & \hat{r_y} & \hat{r_z} \end{pmatrix} \quad (1.28)$$

Multiplication of these two vectors gives a 3x3 matrix whose elements correspond to the coefficients of diffusion constants in the lab frame in Equation 1.27.

$$\mathbf{b} = b \begin{pmatrix} \hat{r_x}^2 & \hat{r_x}\hat{r_y} & \hat{r_x}\hat{r_z} \\ \hat{r_y}\hat{r_x} & \hat{r_y}^2 & \hat{r_y}\hat{r_z} \\ \hat{r_x}\hat{r_y} & \hat{r_z}\hat{r_y} & \hat{r_z}^2 \end{pmatrix} \quad (1.29)$$

Then, simple version of signal intensity $E(\mathbf{b})$ in Equation 1.27 is given by

$$E(\mathbf{b}) = \exp\left(-\sum_{i=1}^{3}\sum_{j=1}^{3} b_{ij}D_{ij}\right) \quad (1.30)$$

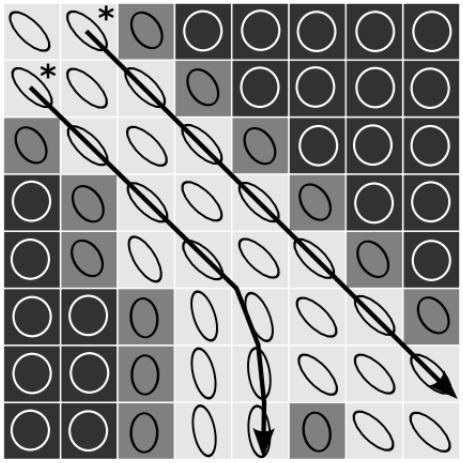

Figure 1.8. Fiber tracking starts at two different voxels and connections with principal eigenvectors follow different pathways. FA value is displayed with gray colour [3].

A new scalar quantity is described to measure the degree of anisotropy of diffusion process, which utilizes the eigenvalues of the measured tensor. It is mostly described as Fractional Anisotropy (FA) [33, 34], which is calculated by the following equation:

$$FA = \sqrt{\frac{3\left[(\lambda_1 - \langle\lambda\rangle)^2 + (\lambda_2 - \langle\lambda\rangle)^2 + (\lambda_3 - \langle\lambda\rangle)^2\right]}{2(\lambda_1^2 + \lambda_2^2 + \lambda_3^2)}} \tag{1.31}$$

where $\langle\lambda\rangle$ is another scalar quantity so called mean diffusivity, which is the average value of ADC along three orthogonal directions.

$$\langle\lambda\rangle = \frac{\lambda_1 + \lambda_2 + \lambda_3}{3} \tag{1.32}$$

FA value is normalized ranging from 0 to 1. If all the eigenvalues are equal (isotropic, FA value is zero. On the other hand, if there is a sharp ratio between the eigenvalues, FA value aproaches to 1 and diffusion is fully restricted.

To determine the neurol connectivity of different parts of the brain, fibre tracking algorithms are utilized. In Figure 1.8, an example of streamline tractography [35] is

shown. Measuring the diffusion tensor for each voxel provides the principal direction of fiber at each voxel. Then it can be deduced that pathway of fiber bundles shows streamline predicted by connecting up the estimated ellipsoids.

1.6. Advantages And Limitations Of Models

In DTI, single-PFG acquisitions at low q-values were employed to characterize the microstructural properties such as orientation of fiber. ADCs can be obtained by utilizing gradients at six different spatial direction provided that to probe the bounderies, diffusion time, Δ, is prolonged. Recent works show that signal decay was not fitted the Stejskal-Tanner equation derived in Equation 1.22 at high q-values. Non-monoexponential behavior is observed in the signal decay at high q-values

Although DTI has ability to map neurol architecture in vivo noninvasively, it has some limitations. It is unable to resolve fiber crossing and kissing within a particular voxel illustrated in Figure 1.9. DTI assumes that Gaussian diffusion takes place in a single compartment within each voxel. Gaussian function gives only one directional maxima and thus, cannot appropriately explain fibers at different orientations within a single voxel. In addition to this, Non-monotonicity in the signal at higher q-regime promises that there exist more than a single compartment within a voxel.

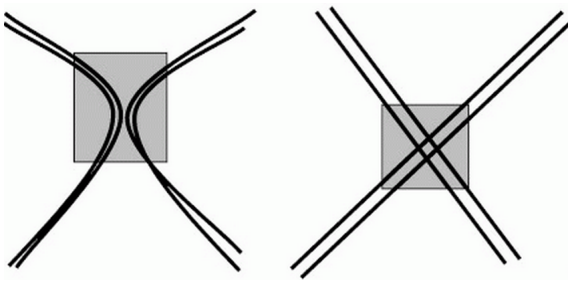

Figure 1.9. Kissing and crossing fibers within a single voxel.

DTI's limitation to resolve multiple fiber bundles within a voxel leads to an alternative approach to investigate the complex systems so called "Q-space imaging" [27,36]. This method is model-free, which does not constraint the process to a Gaussian

function. Local properties are represented as probability distribution functions (PDF) which can be obtained via Fourier relation. Details are given at Section 1.3. In order to resolve fiber crossing, several hundred images are required for reaching high angular resolution. However, this is very time consuming process in comparison with DTI. Only six measurements are necessary for construct the image in DTI. Moreover, high q-values are needed to estimate the compartment size assuming diffusion time, Δ, is adequately long to probe the restricting geometry [37]. Diffusion-diffraction troughs are observed at such q-values [38], which feature structrual information.

In order to overcome such obstacles, a new approach so called "Q-ball imaging (QBI)" is proposed by Tuch [39]. Rather than defining the directional dependence as a diffusion PDF $P(\mathbf{r})$ via Fourier transform as in the case of q-space imaging, orientation distribution function (ODF) $\psi(\theta, \phi)$, radial projection of PDF, is defined for orientational structure of the PDF. Determining ODF is comparably an efficient way in terms of scanning time since radial component is eliminated and fewer gradient sampling is enough to construct the image.

Despite traditional single-PFG methodologies are utilized for observing signal attenuation arising from restricted diffusion, there are some circumstances that its response becomes featureless. For example, a voxel size is much larger than the diameter of an axon, which means it contains thousands of axons with different orientation or size distribution. When taking orientation or size distributions into consideration, single-PFG experiments is unable to obtain axonal properties. To overcome such limitation plays an important role for distinguishing changes in axon radius and orientation. Furthermore, diffusion-diffraction patterns are lost when anisotropic compartments are randomly oriented [1]. Breaking the coherence in the collection of compartments gives rise to a decrease in the anisotropy [40]. In the case that characterization of specimen is quantified by orientation or size distribution, observed anisotropy may disappear when utilizing single-PFG acquisitions. Involving many anisotropic pores with randomly distributed orientations exhibit an isotropic profile, which results in loss of structural information. When the multi-PFG MR sequences are employed, new microstructural information can be gleaned.

Double-PFG sequence as a multi-PFG sequence have been introduced by Cory [41], which is comprised by the addition of two diffusion sensitizing gradient blocks with magnitude of G_1 and G_2 separeted from each other by a mixing time t_m and duration of gradients δ_1 and δ_2 respectively. Spin echo version of such pulse sequence is shown in Figure 1.10.

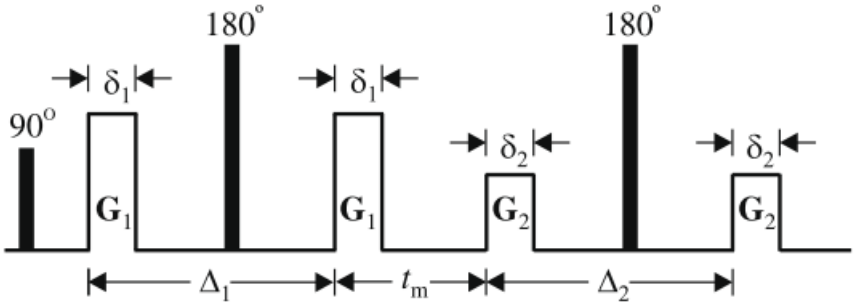

Figure 1.10. Spin echo version of the double-PFG pulse sequence which consists of two PFG blocks $\mathbf{G}_1$, and $\mathbf{G}_2$ with the duration of δ_1 and δ_2 respectively separated by a mixing time t_m. The time between gradient pairs in each block is denoted as diffusion periods, namely, Δ_1 and Δ_2 [4].

Double-PFG experiments are particularly beneficial to differentiate between collection of isotropic pores and randomly distributed elongated pores in the low-q regime while single-PFG experiments are unable to make this distinction as mentioned above. For $\delta \to 0$ (Narrow Pulse Condition) and $\Delta \to \infty$ (enough time to probe the compartment), when the angle ϕ between two gradients $\mathbf{G}_1$ and $\mathbf{G}_2$ is varied, angular dependence of the MR signal intensity has observed even when the shape of pores are spherical [42]. Different range of t_m values facilitate to distinguish these two different ensembles described above from each other. When t_m approaches to zero, angular dependence of the signal intensity can be observed for all compartment shape. Exhibition of such anisotropy provides a mechanism for investigating the effect of restricted diffusion, which is namely called as microscopic anisotropy (μA) [4]. Such anisotropy is observed as a result of restrictive character of boundary of compartment [4, 43]. However, when t_m goes to infinity, dependence of signal intensity on the angle ϕ between gradients holds only for randomly distributed non-spherical compartments. This

observed anisotropy for $t_m \to \infty$ is referred to as compartment shape anisotropy (CSA). Changing the mixing time t_m allows one to separate these two cases from each other. When the anisotropic compartments are coherently oriented, another anisotropy mech-

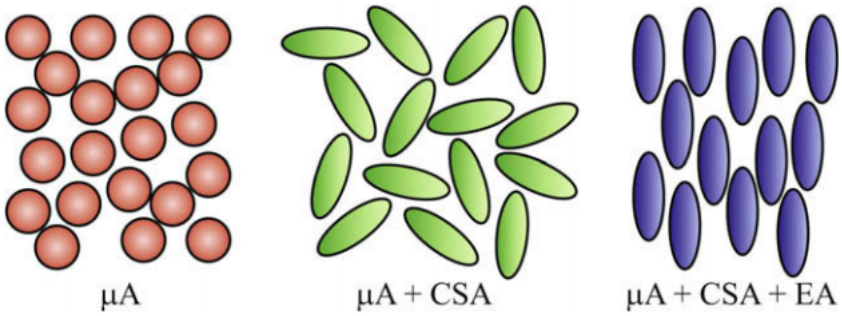

Figure 1.11. Image at the left side represents only μA. Image at the middle shows randomly oriented elongated pores indicating another kind of anisotropy which is compartment shape anisotropy (CSA). Image at the right side exhibits ensembe anisotropy (EA) arising from coherently oriented pores. The image is taken from [4].

anism, ensemble anisotropy (EA), appear. In case of a specimen containing coherently oriented axons, for example, single-PFG experiments are very effective way to exhibit EA. Shematic representation of these 3 anisotropy mechanisms are demonstrated in Figure 1.11 and more details about the mechanisms have been investigated in ref [4].

After theoretical predictions in ref [42], Özarslan proposed exact expressions of the MR signal attenuation resulting from restricted diffusion utilizing double-PFG sequence for arbitrary timing parameters [44]. The multiple correlation function (MCF) formalism [45, 46] is introduced in his work to quantify the effect of restricted diffusion on the NMR signal for simple geometries. To observe the effect of restricted diffusion via double-PFG acquisitions, MCF formalism have been extended to provide variations in the gradient orientation so that one can investigate the signal dependence on the angle between gradients [5]. Moreover, sensitivity of double-PFG sequence enables to probe compartments at low-q regime. Diffusion-diffraction patterns can also be acquired with double-PFG experiments, which allows to estimate the compartment size and eccentricity [47, 48].

2. METHODS

Diffusional behaviour of fluids can be characterized using magnetic resonance (MR) techniques by applying magnetic field gradients into MR pulse sequences to encode the trajectories of spin-bearing particles. In this part we will give an alternative method to observe the effect of the restricted diffusion through obtaining structural information from biological tissue in a useful way. Diffusion-attenuated MR signal for molecules are under the influence of a parabolic potential field is discussed. To account for such effects, the Bloch-Torrey equation [25] is modified by including a new term similar to that in the Smoluchowski operator which is given below.

$$\frac{\partial M(\mathbf{r},t)}{\partial t} = D_0\nabla^2 M(\mathbf{r},t) + D_0\beta\mathbf{f}\nabla\cdot(\mathbf{r}M(\mathbf{r},t)) - i\gamma\mathbf{G}(t)\cdot\mathbf{r}M(\mathbf{r},t) \qquad (2.1)$$

where $M(\mathbf{r},t)$ is the magnetization density, D_0 is the diffusion constant, f is the tensorial spring constant,γ is the gyromagnetic ratio $\beta = \frac{1}{k_b T}$ and $\mathbf{G}(t)$ is the linear magnetic field gradient waveform. Second term on the right hand side of the equation is the parabolic potential term that is added and the last term on the right hand side is the diffusion gradient sensitizing term.

Grebenkov had reformulated the problem of restricted diffusion under inhomogeneous magnetic field for any geometrical confinement which is called multiple correlation function (MCF) framework [46]. MCF method is based on solving Bloch-Torrey equation by introducing matrix formalism. Then Özarslan *et al*. provided the multidimensional generalization of this framework [5]. This extended version of the formalism allows us to incorporate the effects caused by the variations in the orientation of the applied magnetic field gradient so that we can characterize the anisotropy in the NMR signal. The other method that incorporates the effect of restricted diffusion is multiple propagator (MP) framework, which discretizes general gradient waveforms. This reduces the problem to a path integral and analytical expression of the signal can be

obtained for general gradient waveforms. Differences and similarities between these two methods were studied in Ref [49].

2.1. Multiple Correlation Function (MCF) Formalism

In this part, I am going to present how the signal intensity is estimated using MCF method.

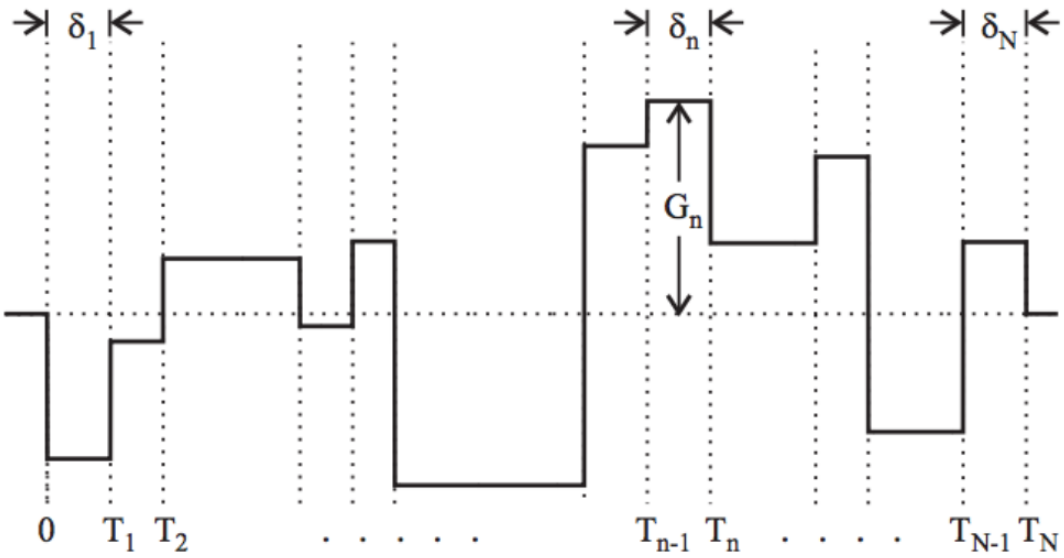

Figure 2.1. A general piecewise-constant gradient waveform $G(t)$ with N intervals is shown [5].

We use MCF method to observe the effect of restricted diffusion. The general gradient waveform is considered as a piecewise-constant function. Such a waveform is broken into succesive different time intervals with different magnitude of gradient G_n in Figure 2.1. For example, G_n is applied between T_n and T_{n-1} interval with a duration of δ_n. Note that the effect of all rf pulses is included in such waveform which means this is the effective gradient profile. Signal intensity for the NMR is expressed as matrix operators.

2.2. Diffusion in Parabolic Potential

Without potential term, Equation 2.1 can be solved using the eigenspectrum of the Laplacian operator, which obeys the Helmholtz equation. When the parabolic potential is introduced into the Bloch-Torrey equation, Laplace operator transforms to Smoluchowski operator , L^2, which is denoted by

$$L^2 = \nabla^2 + D_0\beta\mathbf{f}\nabla\mathbf{r} \tag{2.2}$$

Then, the magnetization of brownian motion under such potential can be rewritten as

$$\frac{\partial M(\mathbf{r},t)}{\partial t} = D_0 L^2 M(\mathbf{r},t) - i\gamma\mathbf{G}(t)\cdot\mathbf{r}M(\mathbf{r},t) \tag{2.3}$$

Noting that the potential is

$$V(\mathbf{r}) = \frac{1}{2}\mathbf{r}^T\mathbf{f}\mathbf{r} \tag{2.4}$$

We have defined the kth eigenfunction $u_k(\mathbf{r})$ which satisfies the Smoluchowski equation

$$L^2 u_k(\mathbf{r}) = -\lambda_k u_k(\mathbf{r}) \tag{2.5}$$

Eigenfunctions $u_k(\mathbf{r})$ form a complete basis. Hence we can expand $M(\mathbf{r},t)$

$$M(\mathbf{r},t_n) = \sum_{k'} b_{k'}(t_n)u_{k'}(\mathbf{r}) \tag{2.6}$$

Total time is discretized into small intervals and the subscript n indicates n-th time interval, i.e., $T_{n-1} \leq t \leq T_n$. $\mathbf{G}$ is constant for all time interval, and will be represented as $\mathbf{G}_n$. Inserting above expansion into Equation 2.3 and multiplying by $w_k(\mathbf{r})$ and integrating over $\mathbf{r}$ results in the expression

$$\frac{\partial b_k}{\partial t_n} = -\sum_{k'} b_{k'}(t_n)\Lambda_{kk'} - i\gamma \mathbf{G}_n \cdot \sum_{k'} b_{k'}(t_n)\mathbf{A}_{kk'} \tag{2.7}$$

where infinite dimensional operator $\Lambda_{kk'}$ is equal to

$$\Lambda_{kk'} = \beta f D_0 k \delta_{kk'} \tag{2.8}$$

Moreover, elements of the vector operator $\mathbf{A}_{kk'}$ is given by

$$\mathbf{A}_{kk'} = \int d\mathbf{r} w_k(\mathbf{r}) \mathbf{r} u_{k'}(\mathbf{r}) \tag{2.9}$$

As a result, evolution equation in Equation 2.7 becomes

$$b(t_n) = e^{-(\Lambda + i\gamma \mathbf{G}_n \cdot \mathbf{A})(t_n - T_{n-1})} b(T_{n-1}) \tag{2.10}$$

describing the time evolution of the magnetization within nth interval $T_{n-1} \leq t_n \leq T_n$. With the choice of $t_n = T_N$ and denoting $\delta_n = T_n - T_{n-1}$, and

$$q_n = (2\pi)^{-1} \gamma \delta_n G_n \tag{2.11}$$

Equation 2.10 is a recurrence equation :

$$b(T_n)^* = b(0)^* \prod_{n=1}^{N} e^{-\Lambda \delta_n + i 2\pi q_n A^*}. \tag{2.12}$$

Hermitian conjugate of the preceding expression comes from the fact that pulse sequences that are applied later are expressed right of the earlier pulses. When a system reaches equilibrium, its magnetization density approaches Boltzman distribution. When the Dirac's bra-ket notation is employed, magnetization density in equilibrium

state is written as

$$E = \int d\mathbf{r} M(\mathbf{r}, T_N) = \int d\mathbf{r} < \mathbf{r}| \prod_{n=1}^{N} e^{-\Lambda\delta_n + i2\pi q_n A^*} |b(0)^* > \tag{2.13}$$

Using the orthonormaity and completeness relations given below

$$\langle w_k | u_k \rangle = \int d\mathbf{r} u_k(\mathbf{r}) w_{k'}^*(\mathbf{r}) = \delta_{k'k} \tag{2.14}$$

$$\sum_k |u_k >< w_k| = 1 \tag{2.15}$$

NMR signal in Equation 2.13 can be rewritten

$$E = \sum_{k,k'} \int d\mathbf{r} < \mathbf{r}|u_k >< w_k|\mathbf{U}(t,0)|u_{k'} >< w_{k'}|b(0)^* > \tag{2.16}$$

where $U(t,0)$ is the Green's function. As indicated above, when there is no any applied gradient, magnetization density is in the equilibrium state and proportional to zeroth eigenvalue. Then, the corresponding eigenfunction is equal to Boltzman distribution given below with the normalization constant Z

$$u_0(\mathbf{r}) = \frac{1}{\sqrt{Z}} e^{-\beta V(\mathbf{r})} \tag{2.17}$$

With the help of orthonormality relation, one can find the $w_0(\mathbf{r})$ as

$$w_0(\mathbf{r}) = \frac{1}{\sqrt{Z}} \tag{2.18}$$

inserting $\langle w_{k'}|b^*(0)\rangle = \delta_{k'0}$ and $\int d\mathbf{r} \langle \mathbf{r}|u_k\rangle = \delta_{0k}$ into the signal expression in Equation 2.16, one can simply write

$$E = \langle w_0|\mathbf{U}(t,0)|u_0\rangle =< w_0| \prod_{n=1}^{N} e^{-\Lambda\delta_n + i2\pi q_n A^*} |u_0 > \tag{2.19}$$

Total MR signal attenuation is the first element of the resultant matrix, which is directly related to the operators Λ and $\mathbf{A}$.

2.3. Solving Bloch-Torrey equation with a Parabolic Potential in One Dimension

Bloch-Torrey equation with parabolic potential is written as

$$\frac{\partial M(x,t)}{\partial t} = D_0 \frac{d^2 M(x,t)}{dx^2} + \beta f D_0 \frac{d}{dx}(xM(x,t)) - i\gamma G(t) x M(x,t) \tag{2.20}$$

One can find the the eigenvalues and eigenfunctions of the Smoluchowski equation in 2.5. Eigenfunctions are as follows:

$$u_k(x) = a_k e^{-\beta f x^2/2} H_k\left(\sqrt{\frac{\beta f}{2}} x\right) \tag{2.21}$$

with the eigenvalues of

$$\lambda_k = k\beta f D_0 \qquad (k = 0, 1, 2, ...) \tag{2.22}$$

The term $H_k(x)$ in the eigenfunction of $u_k(x)$ in Equation 2.21 is the Hermite polynomials and a_k is a normalization constant. The eigenfunctions of the Smoluchowski operator obey the orthogonality property

$$\int_{-\infty}^{+\infty} d\xi e^{\xi^2} H_k(\xi) H_{k'}(\xi) = 2^k k! \sqrt{\pi} \delta_{kk'} \tag{2.23}$$

After changing variable, $u_k(x)$ is choosen to be

$$u_k(x) = \sqrt{\frac{\beta f}{2\pi}} \frac{1}{2^k k!} e^{-\beta f x^2/2} H_k\left(\sqrt{\frac{\beta f}{2}} x\right) \tag{2.24}$$

and defining

$$w_k(x) = H_k\left(\sqrt{\frac{\beta f}{2}}x\right) \tag{2.25}$$

Normalization constant a_k can be found as

$$a_k = \sqrt{\frac{\beta f}{2\pi}}\frac{1}{2^k k!} \tag{2.26}$$

Additionally, magnetization density is initially in the equilibrium state, which obeys Boltzman distribution. So initial magnetization $M(x,0)$ is equal to

$$M(x,0) = \sqrt{\frac{\beta f}{2\pi}}e^{-\beta f x^2/2} \tag{2.27}$$

The coefficient of exponential term is normalization factor. Next step is to calculate elements of vector operator **A**. One dimensional version of Equation 2.9 is

$$A_{kk'} = \int dx w_k(x) x u_{k'}(x) \tag{2.28}$$

Substituting the eigenfunctions $w_k(x)$ and $u_{k'}(x)$ into the above equation

$$A_{kk'} = \sqrt{\frac{\beta f}{2\pi}}\frac{1}{2^{k'}k'!}\int dx H_{k'}\left(\sqrt{\frac{\beta f}{2}}x\right) x H_k\left(\sqrt{\frac{\beta f}{2}}x\right) e^{-\beta f x^2/2} \tag{2.29}$$

One can evaluate the matrix element $A_{kk'}$

$$A_{kk'} = \sqrt{\frac{1}{\beta f}}\frac{2^{(k-k')/2}k!}{(\frac{k'-k+1}{2})!(\frac{k-k'+1}{2})!(\frac{k'+k-1}{2})!} \tag{2.30}$$

provided that $k + k'$ is odd, $|k - k'| = 1$ otherwise $A_{kk'} = 0$.
If solutions of these two operators are inserted into Equation 2.19, MR signal attenuation can be acquired from a piecewise-constant gradient waveform.

2.4. Path Integral Formalism in One Dimension

We use gradient waveforms to sensitize the MR signal to the diffusional motion of molecules so that we can obtain information about microstructure of the biological tissue. Molecules are diffusing in the presence of gradient $\mathbf{G}(t)$ and some net phase shift is induced

$$\phi = -\gamma \int \mathbf{G}(t) \cdot \mathbf{r}(t) dt \tag{2.31}$$

where $\mathbf{r}(t)$ is the position of a molecule in the direction of applied gradient $\mathbf{G}(t)$. Spin bearing particles with different position experience different magnetic field. As a result each particle picks up different phase. So there is a distribution of phases and echo amplitude is given by

$$E = \left\langle e^{i\phi} \right\rangle = \left\langle e^{-i\gamma \int_0^T dt \mathbf{G}(t) \cdot \mathbf{r}(t)} \right\rangle \tag{2.32}$$

Noting that T is the duration of the magnetic field gradient $\mathbf{G}$ and E is a normalized quantity. Because the average signal intensity is to be taken over all random paths $\mathbf{r}(t)$, the expectation value has the form of a path integral. Any gradient pulse is dicretized to infinitesimally narrow pulses with initial spin magnetization distribution $\rho(\mathbf{r}_1)$. Here, we derive analytical expression for the MR signa under parabolic potentials using path integral. Path integral equation in one dimension is

$$E = \int dx_0 \rho(x_0) e^{-iq_0 x_0} \int dx_1 P_\tau(x_0, x_1) e^{-iq_1 x_1} \int dx_2 ... \int dx_m P_\tau(x_{m-1}, x_m) e^{-iq_m x_m} \tag{2.33}$$

where $q_j = (2\pi)^{-1} \gamma \delta_j G_j$ which is indicated in Equation 2.11. This equation states that molecules starts to diffuse from initial position $x_1 = x_1(\tau)$ with the probability density $\rho(x_0)$ to the subsequent positions x_1,x_2,...x_m with corresponding probability densities $P_\tau(x_0, x_1)$,$P_\tau(x_1, x_2)$,...$P_\tau(x_{m-1}, x_m)$. Such integral can be written as closed form

$$E = \int dx_0 \rho(x_0) e^{-iq_0 x_0} \prod_{j=1}^{m} dx_j P_\tau(x_{j-1}, x_j) e^{-iq_j x_j} \tag{2.34}$$

Here, the time interval $0 < t < T$ can be divided into a number of m subintervals of duration $\tau = \frac{T}{m}$ and t is replaced by $j\tau$ for the discretization. The propagator for diffusion under parabolic potential $V(x) = \frac{1}{2}fx^2$ is found as

$$P_t(x_a, x_b) = \frac{1}{\sqrt{2\pi\sigma_t^2}} e^{-\frac{(x_b - s_t x_a)^2}{2\sigma_t^2}} \tag{2.35}$$

where s_t and σ_t^2 are

$$s_t = e^{-\Omega t} \tag{2.36}$$

$$\sigma_t^2 = (1 - s_t^2)\frac{D}{\Omega} \tag{2.37}$$

defining the inverse time Ω as

$$\Omega = \frac{fD}{k_b T} \tag{2.38}$$

Each integrals in Equation 2.33 are nothing but the Fourier transform of the probability densities or the propagator. In order to solve Equation 2.33, you need to start from outer-most integral to the inner-most integral since there will be contribution from the last integrand to the previous one. So Fourier transform of the outer-most propagator is given by

$$\int dx_m P_\tau(x_{m-1}, x_m) e^{-iq_m x_m} = e^{-\frac{1}{2}\sigma_\tau^2 q_m^2} e^{-ix_{m-1} s_\tau q_m} \tag{2.39}$$

Then the next integral with the solution of outer-most one is

$$\int dx_{m-1} P_\tau(x_{m-2}, x_{m-1}) e^{-iq_{m-1} x_{m-1}} e^{-\frac{1}{2}\sigma_\tau^2 q_m^2} e^{-ix_{m-1} s_\tau q_m} \tag{2.40}$$

after rearranging Equation 2.40

$$e^{-\frac{1}{2}\sigma_\tau^2 q_m^2} \int dx_{m-1} P_\tau(x_{m-2}, x_{m-1}) e^{-ix_{m-1}(q_{m-1}+s_\tau q_m)} \tag{2.41}$$

using the identity in Equation 2.39 and replace $q_{m-1} + s_\tau q_m$ instead of q_m, solution is

$$e^{-\frac{1}{2}\sigma_\tau^2(q_m^2+(q_{m-1}+s_\tau q_m)^2)} e^{-ix_{m-2}s_\tau(q_{m-1}+s_\tau q_m)} \tag{2.42}$$

This solution combines with the next integral and goes like that. Exponent of the first factor in Equation 2.39 grows up in the following fashion:

$$\frac{1}{2}\sigma_\tau^2 q_m^2 \tag{i}$$

$$\frac{1}{2}\sigma_\tau^2 \left\{q_m^2 + (q_{m-1} + s_\tau q_m)^2\right\} \tag{ii}$$

$$\frac{1}{2}\sigma_\tau^2 \left\{q_m^2 + (q_{m-1} + s_\tau q_m)^2 + (s_\tau^2 q_m + s_\tau q_{m-1} + q_{m-2})^2\right\} \tag{ii}$$

If one defines

$$Q_j = \sum_{i=j}^{m} s_\tau^{i-j} q_i \tag{2.43}$$

Then, the path integral equation in Equation 2.33 can be written as

$$E = e^{-\frac{1}{2}\sigma_\tau^2 \sum_{j=1}^{n} Q_j^2} \int dx_0 \rho(x_0) e^{-iQ_0 x_0} \tag{2.44}$$

In the limit that time t goes to infinity, initial spin magnetization density $\rho(x_0) = P_\infty$ and remaining integral in Equation 2.44 can be calculated similarly with the previous

integrations. So Equation 2.44 becomes

$$E = e^{-\frac{1}{2}\sigma_\tau^2 \sum_{j=1}^{n} Q_j^2 - \frac{1}{2}\sigma_\infty^2 Q_0^2} \tag{2.45}$$

When the time t goes to infinity, σ_∞^2 is $\frac{D}{\Omega}$ via Equation 2.37

$$E = \exp\left\{-\frac{D}{2\Omega}(1 - e^{-2\Omega\tau})\sum_{j=1}^{m} Q_j^2 - \frac{D}{2\Omega}Q_0^2\right\} \tag{2.46}$$

In order to make a transition from discrete version to continuum one, we need to look at the continuum limit where the duration of subinterval $\tau = \frac{T}{m}$ goes to zero when the number of subintervals m goes to infinity. In the limit that the $\tau \to 0$, above expression can be written as

$$E = \exp\left\{-D\int_0^T dt Q^2(t) - \frac{D}{2\Omega}Q^2(0)\right\} \tag{2.47}$$

Noting that $q_j = \tau\gamma G(j\tau)$. Using the expression in Equation 2.36, Q_j becomes the following

$$Q_j = \gamma\tau\sum_{i=j}^{m} G(j\tau)e^{-\Omega\tau(i-j)} \tag{2.48}$$

In the continuum limit that $\tau \to 0$ one finds

$$Q(t) = \gamma\int_t^T dt' e^{-\Omega\tau(t'-t)}G(t') \tag{2.49}$$

2.5. Path Integral Formalism in Three Dimension

In this part, multidimensional generalization of the results in Equation 2.47 and Equation 2.49 will be implemented. Harmonic potential in three dimensions can be

written as

$$V(\mathbf{r}) = \frac{1}{2}\sum_{i=1}^{3} f_i r_i^2 = \frac{1}{2}f_1 x^2 + \frac{1}{2}f_2 y^2 + \frac{1}{2}f_3 z^2 \tag{2.50}$$

assuming that f_1,f_2 and f_3 are the eigenvalues of the stiffness tensor f_{ij} since f_{ij} is diagonal.

$$P_t(\mathbf{r}_a, \mathbf{r}_b) = \prod_{i=1}^{3} \frac{1}{\sqrt{2\pi\sigma_{t,i}^2}} exp\left\{-\frac{(\mathbf{r}_{b,i} - s_{t,i}\mathbf{r}_{a,i})^2}{2\sigma_t^2}\right\} \tag{2.51}$$

where $s_{t,i}$ and $\sigma_{t,i}^2$ are the following

$$s_{t,i} = e^{-\Omega_i t} \tag{2.52}$$

$$\sigma_{t,i}^2 = (1 - s_{t,i}^2)\frac{D}{\Omega_i} \tag{2.53}$$

Noting that the inverse time Ω_i is

$$\Omega_i = \frac{f_i D}{k_B T} \tag{2.54}$$

Analytical expression of the signal attenuation for harmonic potential in three dimensions can be written as

$$E = \prod_{i=1}^{3} \exp\left\{-D\int_0^T dt Q_i^2(t) - \frac{D}{2\Omega_i}Q_i^2(0)\right\} \tag{2.55}$$

where $Q_i(t)$ is

$$Q_i(t) = \gamma \int_t^T dt' e^{-\Omega_i \tau(t'-t)} G_i(t') \tag{2.56}$$

2.6. Results

Magnetization arising from molecules under the influence of parabolic potential can be obtained by using a piecewise-constant gradient waveform via MCF framework which is given in Equation 2.19. Open form of NMR signal attenuation from single-PFG waveform drawn in Figure 1.2 is simply written as a product of operators represented by matrix exponentials

$$E = \langle 0| \, e^{-\Lambda\delta + i2\pi\mathbf{q}\cdot\mathbf{A}^\dagger} e^{-\Lambda(\Delta-\delta)} e^{-\Lambda\delta + i2\pi\mathbf{q}\cdot\mathbf{A}^\dagger} \, |0\rangle^* \quad . \tag{2.57}$$

Logarithmic plot of the signal intensity $E(q)$ in the simulation of single-PFG (Stejskal-Tanner pulse) experiment is plotted against q-values in Figure 2.2 for the pulsed gradient duration δ values of 20ms, 12ms, 5ms and 1ms respectively from upper curve (green) to lower one (red). The dashed curve represents Stejskal's result derived in Equation 1.17 which is valid for delta-shape gradient pulses. When the narrow

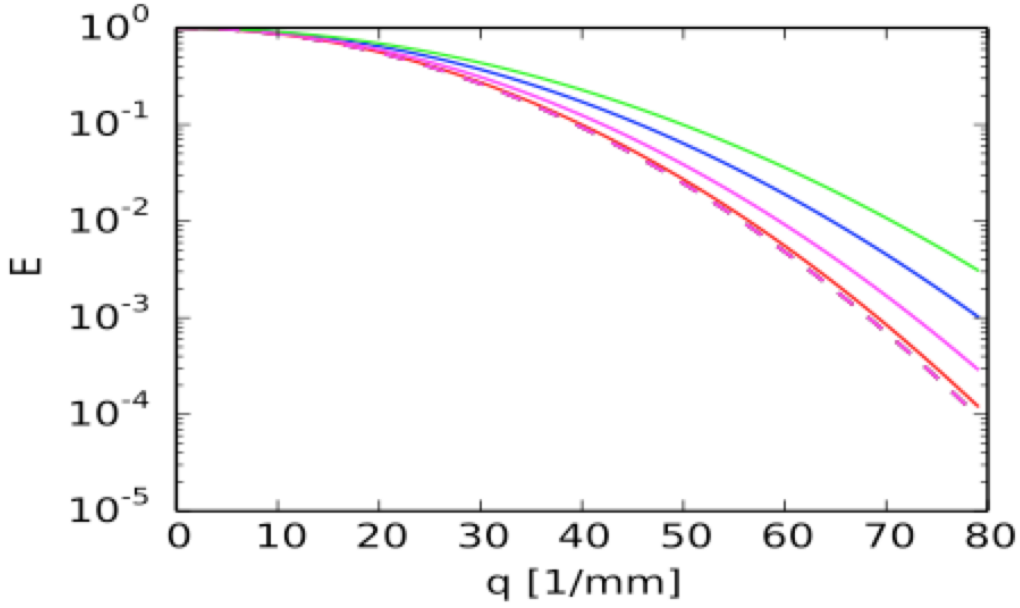

Figure 2.2. MR signal is plotted as a function of q for different pulse durations (δ) of the single-PFG sequence. Diffusion time Δ=60ms. Green: δ=20ms, Blue: δ=12, Pink: δ=5ms, Red: δ=1ms.

gradient pulses ($\delta \to 0$) are applied, signal attenuation converges to Stejskal's result for the case of traditional PFG sequences featuring one pair of infinitesimal pulses. Narrow gradient pulse approximation enables a validation for our solution of the problem.

In Figure 2.3, logarithmic plot of signal intensity $E(q)$ is plotted against the q-value again but for different θ values of 90°, 60°, 30° and 0° where θ is the angle between the gradient vector and the z-axis when the principal spring constants satisfy the condition $f_z < f_x = f_y$. Fulfilling this requirement provides one to construct a cylindrical geometry such as axons. Molecules are moving freely in the z-axis in comparison with that in the other axes since principal spring constant in the z-axis is relatively small. Thus, the effective stiffness is reduced as the gradient direction approaches 0°. Morever, when the direction of the gradient is changed, different signal attenuation profile is observed. These results indicate that anisotropic potentials provide an alternative mechanism for the observed diffusion anisotropy.

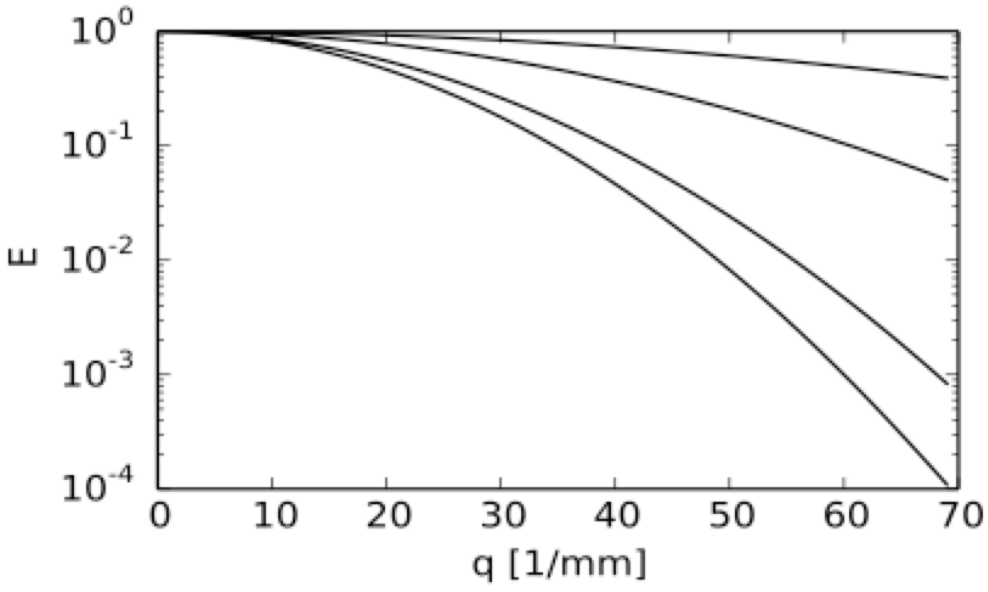

Figure 2.3. MR signal for coherently oriented anisotropic springs is shown for increasing q-values. Each curvature represents θ values of 90°, 60°, 30° and 0° from top to bottom.

An angular dependence of the NMR diffusion signal is also observed when a double-PFG experiment demonstrated in Figure 1.10 is conducted on a system involving many springs with randomly distributed orientations. In case of $\delta = \delta_1 = \delta_2$ and $\Delta = \Delta_1 = \Delta_2$, signal expression for the double-PFG sequences is given by

$$E = \langle 0 | \, e^{-\Lambda\delta + i2\pi\mathbf{q}_1\cdot\mathbf{A}^\dagger} e^{-\Lambda(\Delta-\delta)} e^{-\Lambda(t_m-\delta)} e^{-\Lambda\delta - i2\pi(\mathbf{q}_1+\mathbf{q}_2)\cdot\mathbf{A}^\dagger} e^{-\Lambda\delta + i2\pi\mathbf{q}_2\cdot\mathbf{A}^\dagger} \, |0\rangle^* \ . \qquad (2.58)$$

The experiment is performed with a fixed $\mathbf{q}$ value, which is the same for both pairs of gradients. Moreover, $\mathbf{G}_1$ is fixed in a certain direction, but the direction of $\mathbf{G}_2$ is changed relative to $\mathbf{G}_1$ by an angle ϕ. In Figure 2.4, signal intensity is plotted as a function of ϕ for such angular double-PFG experiments with four different t_m (mixing time) values of 60 ms, 6 ms, 0.6 ms and 0.006 ms. A smooth transition from a nearly bell-shaped modulation (red curve) to a w-shaped modulation (violet) is observed when t_m is prolonged as is the case for restricted diffusion [4] mentioned in Section 1.6. These results suggest the sensitivity of the double-PFG technique to the the local anisotropy of the potential field.

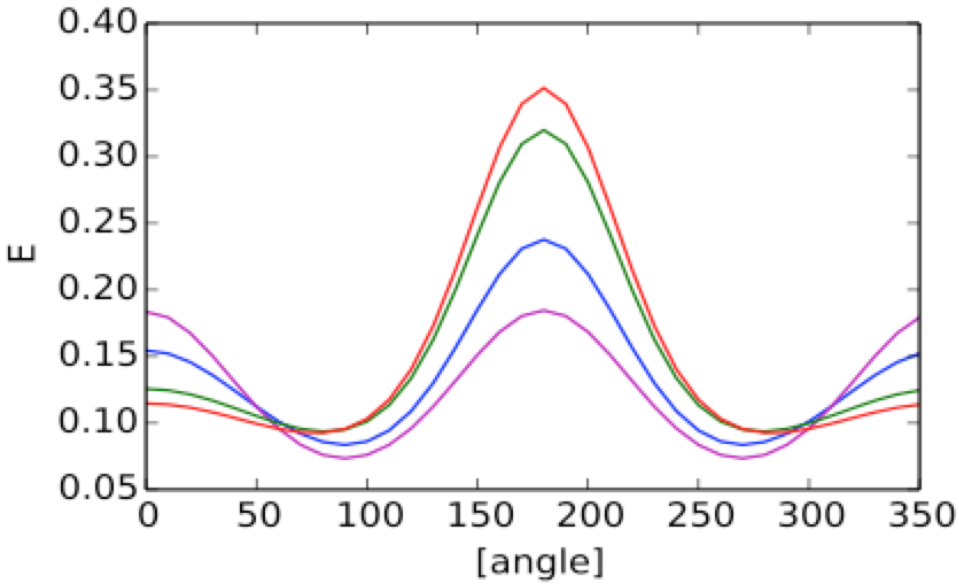

Figure 2.4. Double-PFG signal profiles for randomly distributed anisotropic springs plotted against the angel (in degrees) between the two gradients of the sequence for different values of the mixing time, t_m. Red: t_m=6 μs, Green: t_m=0.6 ms, Blue t_m=6 ms and Violet: t_m= 60 ms.

3. ROTATING FIELD GRADIENT (RFG) AS A NEW SENSITIZATION MECHANISM

Diffusion-weighted magnetic resonance imaging (MRI) is an excellent way to map the white matter fiber connectivity in the central nervous system in vivo and noninvasively. Structural information about the underlying tissue is achieved by sensitizing the MRI signal to diffusion. Displacement of water molecules are measured to charactrerize the tissue. When the molecules are moving isotropically without encountering any boundaries, displacement probability distribution is a Gaussian distribution. However, cells are very crowded places that contain membranes, macromolecules and organelles in which displacement of molecules can be exposed to a barrier effect modifying the probability distribution fucntion (PDF). As indicated in Section 1.5, DTI is very impressive technique to probe the tissue microstructure, which is based on anisotropic Gaussion probality distribution [15]. In case of multiple fiber orientations within a voxel, DTI method fails since it gives only one directional maxima within each voxel. To overcome this limitation of DTI, several methods have been suggested to resolve the fiber orientations [39, 50–54]. Q-space imaging [27] and Q-ball imaging [39] are two of the such proposed methods for measuring PDF to distinguish multiple fiber directions.

Such methods mentioned above are based on Stejskal-Tanner pulse sequences featuring one pair of gradients [26]. Signal attenuation arising from applying such traditional PFG sequences is simply coverted to PDF thorugh a Fourier relationship. Recently, more sophisticated pulse sequences are introduced for getting improved orientational sensitivity. Rotating field gradient (RFG) [55, 56] MR is the most interested one for mapping neurol connectivity.

An RFG pulse can be generated by simultaneously applying sine- and cosine modulated gradient waveforms along two perpendicular directions with 90° phase shift between them around 180° RF refocusing pulse in a spin echo sequence, which yields rank-2 **b** matrices (See: Figure 3.1). When the RFGs are performed with varying the

axis of rotation, orientation at which the maximum signal value is observed coincides with the orientation where the maximum diffusivity takes place. When this effect is taken into consideration for all compartments within voxel, the aggregate signal can be represented as the diffusion orientation distribution function (dODF). Therefore, requirement of transforming the signal into the displacement space is obviated conveniently.

In this part, the RFG responses of both DTI model and the model proposed in this thesis (MR signal under the influence of a Hookean force) are investigated for various b-values and compare the results with QBI [39] (PFG based method) and its extension to constant solid angle (CSA) [53].

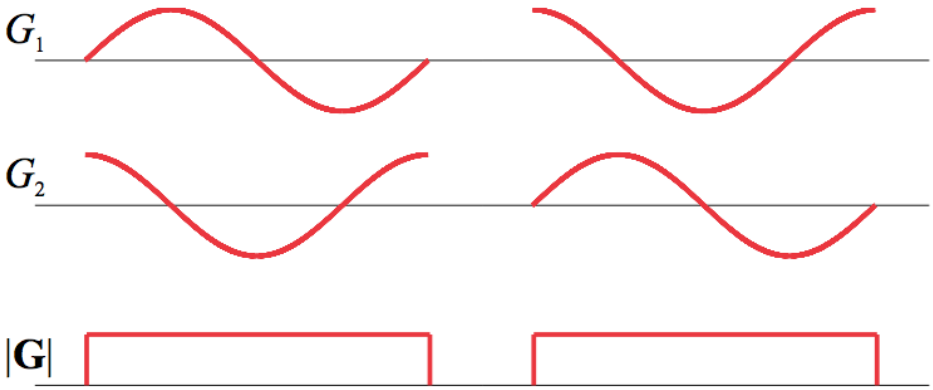

Figure 3.1. First two rows: An RFG pulse comprises two oscillating gradient waveforms around 180° RF pulse with 90° phase shift applied simultaneously two orthogonal directions. Bottom row: Vector sum of the RFG pulse sequence is nothing but the traditional Stejskal-Tanner pulse.

3.1. Calculation of Signal Expression for Free Diffusion

Signal expression for free diffusion is derived in Equation 1.30. When randomly oriented N anisotropic, Gaussian compartments in the voxel are considered, signal expression is given by

$$E(\mathbf{b}) = \sum_{n=1}^{N} f_n \exp[-\mathbf{b} : \mathbf{D}^{(n)}] \tag{3.1}$$

where f_n corresponds to the signal fraction for the nth compartment and Einstein summation convention is employed for shortening the equations, $\mathbf{b} : \mathbf{D}^{(n)} = b_{ij}D_{ij}$. So b-matrix can be calculated for the RFG pulse through changing the relation in Equation 1.20. If $\mathbf{F}$ is defined as $\mathbf{F} = \int_0^t \mathbf{G}(t')dt'$, b-matrix is given by

$$\mathbf{b} = \gamma^2 \int_0^{TE} \left(\mathbf{F}^T\mathbf{F}\right) dt \tag{3.2}$$

The design of G_1 and G_2 describes a plane of rotation whose normal is denoted by $\mathbf{n}$ shown in Figure 3.2. θ is the angle between the n-vector (normal vector) and the z-axis. ϕ is the azimuthal angle of the n-vector.

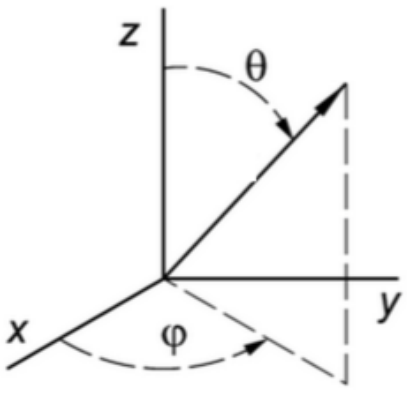

Figure 3.2. Representation of a vector in cartesian coordinate system where θ is the angle between the vector and z-axis and ϕ is the azimuthal angle.

For the sake of simplicity, θ is equal to zero so that rotation takes place on the xy plane. Since there is no gradient in the z-axis for this case, contribution from the z-component of the gradient vanishes. Thus, gradient vector for the RFG pulse sequnence before the addition of 90° (See: Figure 3.1) can be written as

$$\mathbf{G}_0 = G \begin{pmatrix} \sin(\phi)\sin(\phi - \omega t - \phi_0) + \cos(\phi)\cos(\phi - \omega t - \phi_0) \\ -\cos(\phi)\sin(\phi - \omega t - \phi_0) + \sin(\phi)\cos(\phi - \omega t - \phi_0) \end{pmatrix} \tag{3.3}$$

After introducing 90° phase shift with 180° RF pulse, the gradient vector can be written as

$$\mathbf{G}_{\frac{\pi}{2}} = G \begin{pmatrix} -\sin(\phi)\cos(\phi - \omega(t - t_m) - \phi_0) + \cos(\phi)\sin(\phi - \omega(t - t_m) - \phi_0) \\ \cos(\phi)\cos(\phi - \omega(t - t_m) - \phi_0) + \sin(\phi)\sin(\phi - \omega(t - t_m) - \phi_0) \end{pmatrix} \tag{3.4}$$

where subscripts in the $\mathbf{G}_0$ and $\mathbf{G}_{\frac{\pi}{2}}$ represent the gradient before and after involving 90° respectively and G is the gradient magnitude. $\mathbf{G}_{\frac{\pi}{2}}$ contains t_m which is the time difference between RFG pairs. Note that ϕ_0 is the starting phase of the experiment. Components of $\mathbf{b}$ matrix can be obtained by using Equation 3.2 and given by

$$b_{xx} = b_{yy} = \frac{4\pi(\gamma G)^2}{\omega^3} \tag{3.5}$$

All other components of $\mathbf{b}$ matrix vanish. In other words, components of the matrix can be given by

$$b_{ij} = \frac{4\pi(\gamma G)^2}{\omega^3}(\delta_{ix}\delta_{jx} + \delta_{iy}\delta_{jy}) \tag{3.6}$$

where δ is the Kronecker delta and ω is the angular frequency of rotation. The signal attenuation expression for whole compartments is given by

$$E(\mathbf{b}) = \sum_{n=1}^{N} f_n \exp\left[\frac{4\pi(\gamma G)^2}{\omega^3}(D_{xx}^{(n)} + D_{yy}^{(n)})\right] \tag{3.7}$$

3.2. Calculation of Signal Expression for Restricted Diffusion

Analytical expression of signal attenuation for the case of molecules under the influence of the parabolic potential can be obtained by using multiple propagator approach (See: Section 2) , which is given by

$$E = \exp\left(-D_0 \int_0^T dt|\mathbf{Q}(t)|^2 - \frac{D_0}{2}\mathbf{Q}^T(0)\mathbf{\Omega}^{-1}\mathbf{Q}(0)\right) \tag{3.8}$$

where $\mathbf{Q}(t)$ is

$$\mathbf{Q}(t) = \gamma \int_t^T dt' e^{-\mathbf{\Omega}(t'-t)\mathbf{G}(t')} \tag{3.9}$$

where Ω is the stiffness tensor. Signal attenuation for general gradient waveforms $\mathbf{G}(t)$ can be found by inserting it into the above relations. So in order to get the signal expression for RFG pulse sequence, one must benefit from above relations.

3.3. Results

Multi-compartmental scenario is considered in the simulations. dODFs of the two differently oriented fiber populations are investigated. For the case of free diffusion, eigenvalues of the diffusion tensor was taken to be $\lambda_1 = 2.5\text{x}10^{-3}$ mm2/s, $\lambda_2 = 0.25\text{x}10^{-3}$ mm2/s and $\lambda_3 = 0.25\text{x}10^{-3}$ mm2/s. For the case of restricted diffusion (MR signal under the influence of a Hookean force), eigenvalues of the stiffness tensor was taken to be $\Omega_1 = 10$ 1/s, $\Omega_2 = 100$ 1/s and $\Omega_3 = 100$ 1/s.

In Figure 3.3 , simulations are performed for getting the dODF profiles for different imaging techniques aiming that the comparison of RFG results with the PFG ones will be analyzed. First two columns show the response functions of QBI and QBI-CSA respectively and third column depicts response function of RFG for anisotropic Gaussian diffusion model while the last column, simulations are repeated for the case of RFG again but generalized it to the case of molecules under potential. Note that

QBI and QBI-CSA are PFG-based methods. Analytical formulation is represented by a series of spherical harmonics up to the order l_{max}=8.

It is clear that when b-value is increased, response function images becomes sharper. High angular resolution is reached for the case of RFG. Sharpness obtained from RFG is superior than that of PFG-based models even at clinically achievable b-values. Moreover, dODFs generated by PFG-based methods experience some spurious peaks while dODFs obtained via RFG do not suffer from such artifacts.

There are two differently oriented fibers with the angles of 10° and 70° in the images. Estimation of the ODF peaks via finding local maxima gives the crossing angles of the two fibers for all three methods [57]. As a result, crossing angles extracted from dODFs reveal that RFG offers MR offers improved orientational sensitivity [57] comparing with other methods.

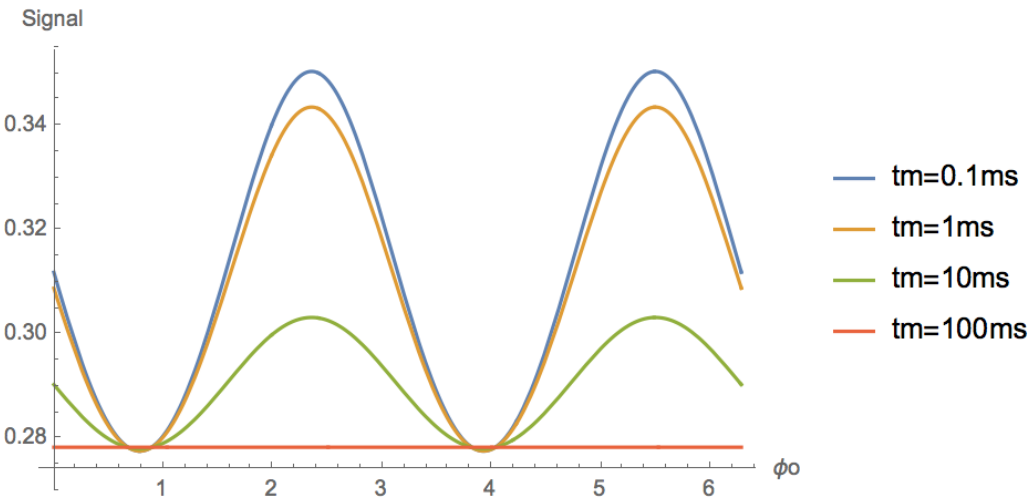

Figure 3.3. Signal intensity obtained from RFG sequence is plotted against ϕ_0 (initial state of the gradient) for different t_m values.

In Figure 3.3, signal intensities are plotted as a function of the initial direction of the gradient vector, ϕ_0, within the plane of rotation for RFG experiments with four different t_m values of 0.1 ms, 1 ms, 10 ms and 100 ms from top to bottom. Anisotropy on the plane of rotation can be detected via RFG experiments at short mixing times with different values for the initial orientation of the vectors.

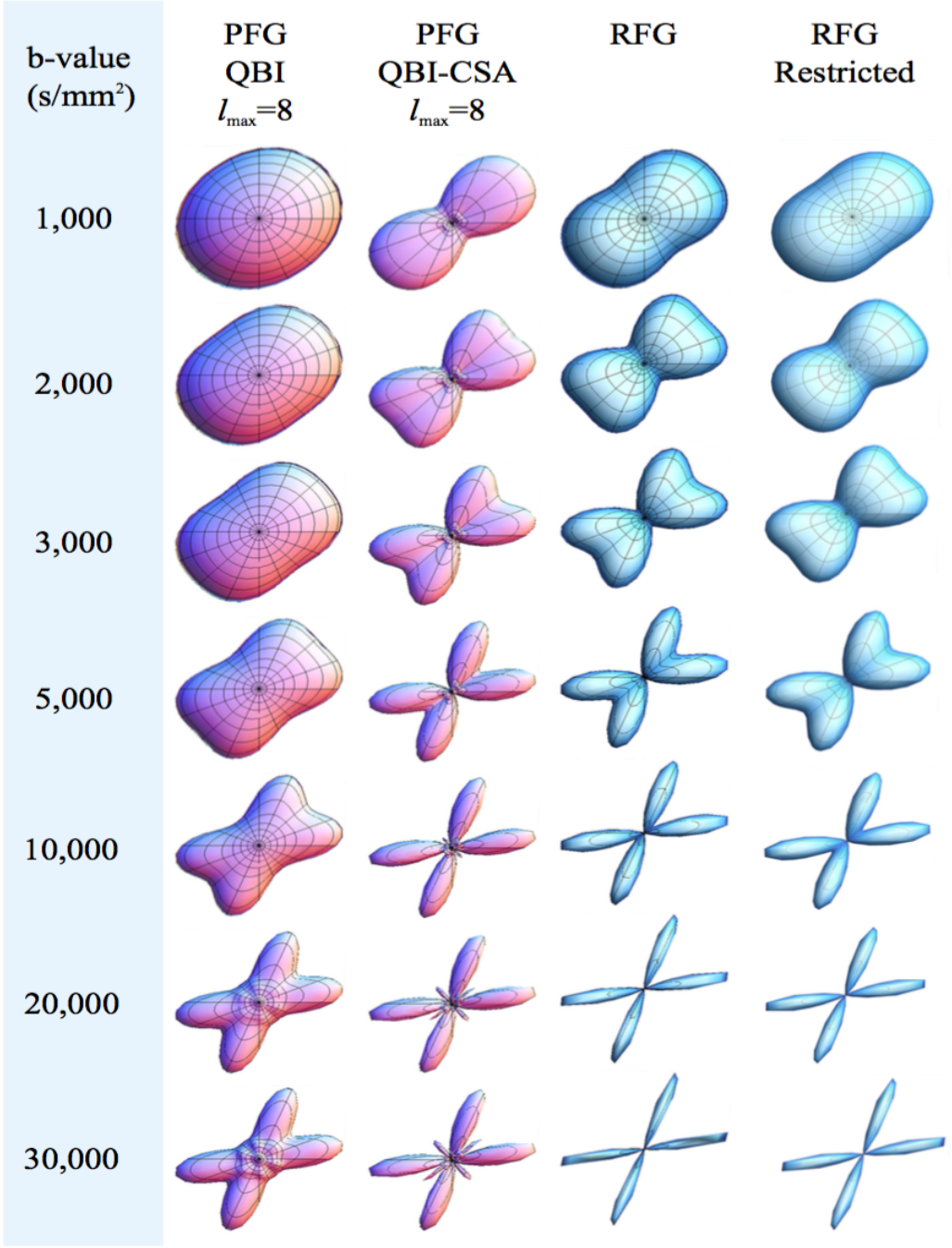

Figure 3.4. Diffusion ODFs for two fibers with crossing angle of 60° are shown for different methods. First two columns show response function of QBI and QBI-CSA. Third column depicts response function of RFG for anisotropic Gaussian while the last one depicts response function of RFG for molecules under the effect of parabolic potential.

4. CONCLUSION

Diffusion MRI is a very promising method that allows to measure the movement of water molecules in biological tissues in vivo, noninvasively. Diffusion process of molecules reflects the microarchitecture of the tissue. Since cellular environment is very complex, moleculer movement is not free but restricted. So change in molecular motion due to the microstructure of the tissue must be correctly revealed by the models. DTI is very effective model that visualize the neural connectivity in the brain. Restriction of molecules by boundaries affect the rate of diffusion in spatial directions and it is described by a diffusion tensor.

Cells in tissue are very crowded places that involves macromolecules, organelles and fibers. MR signal for molecules under the influence of a parabolic potential rather than free potential is considered as more successful model to represent the restricted diffusion. Bloch-Torrey equation was modified by including the potential term to obtain the signal expression. As a result, many features of the MR signal for the case of restricted diffusion are reproduced by molecules diffusing under such potentials. Mathematically more challenging problems about restricted diffusion can be solved approximately by using the solutions for parabolic potential. Further, these results offer why simple harmonic oscillator basis functions are successfully employed for characterizing MR signal [58].

Diffusional behaviour of water molecules can be characterized by using magnetic resonance (MR) techniques by incorporating magnetic field gradients into MR pulse sequences. Involving pulsed field gradients into the spin echo sequences sensitize the signal to diffusion of water molecules. Microstructural features can be revealed by more sophisticated pulse sequences. RFG pulse sequence is one of such pulse sequences that enhanced the orientational sensitivity [57].

RFG-MR is a new sensitization mechanism that employs two gradient vectors applied in perpendicular directions with 90° phase shift thus defining a rotation. RFG

experiments provide a direct measurement of the ODF. At large b-values, such RFG experiments provide a high degree of orientational sensitivity that accurately matches the fiber orientations.

REFERENCES

1. Shemesh, N., E. Özarslan, M. E. Komlosh, P. J. Basser and Y. Cohen, "From Single-pulsed Field Gradient to Double-pulsed Field Gradient MR: Gleaning New Microstructural Information and Developing New Forms of Contrast in MRI", *NMR in Biomedicine*, Vol. 23, No. 7, pp. 757–780, 2010.

2. Mukherjee, P., J. Berman, S. Chung, C. Hess and R. Henry, "Diffusion Tensor MR Imaging and Fiber Tractography: Theoretic Underpinnings", *American Journal of Neuroradiology*, Vol. 29, No. 4, pp. 632–641, 2008.

3. Basser, P. J., S. Pajevic, C. Pierpaoli, J. Duda and A. Aldroubi, "In Vivo Fiber Tractography Using DT-MRI Data", *Magnetic Resonance in Medicine*, Vol. 44, No. 4, pp. 625–632, 2000.

4. Özarslan, E., "Compartment Shape Anisotropy (CSA) Revealed by Double Pulsed Field Gradient MR", *Journal of Magnetic Resonance*, Vol. 199, No. 1, pp. 56–67, 2009.

5. Özarslan, E., N. Shemesh and P. J. Basser, "A General Framework to Quantify the Effect of Restricted Diffusion on the NMR Signal with Applications to Double Pulsed Field Gradient NMR Experiments", *The Journal of Chemical Physics*, Vol. 130, No. 10, p. 104702, 2009.

6. Song, S.-K., S.-W. Sun, W.-K. Ju, S.-J. Lin, A. H. Cross and A. H. Neufeld, "Diffusion Tensor Imaging Detects and Differentiates Axon and Myelin Degeneration in Mouse Optic Nerve After Retinal Ischemia", *Neuroimage*, Vol. 20, No. 3, pp. 1714–1722, 2003.

7. Rugg-Gunn, F. J., S. H. Eriksson, M. R. Symms, G. J. Barker, M. Thom, W. Harkness and J. S. Duncan, "Diffusion Tensor Imaging in Refractory Epilepsy", *The Lancet*, Vol. 359, No. 9319, pp. 1748–1751, 2002.

8. Lee, J. S., M.-K. Han, S. H. Kim, O.-K. Kwon and J. H. Kim, "Fiber Tracking by Diffusion Tensor Imaging in Corticospinal Tract Stroke: Topographical Correlation with Clinical Symptoms", *Neuroimage*, Vol. 26, No. 3, pp. 771–776, 2005.

9. Moffat, B., D. Hall, J. Stojanovska, P. McConville, J. Moody, T. Chenevert, A. Rehemtulla and B. Ross, "Diffusion Imaging for Evaluation of Tumor Therapies in Preclinical Animal Models", *Magnetic Resonance Materials in Physics, Biology and Medicine*, Vol. 17, No. 3-6, pp. 249–259, 2004.

10. Moseley, M., Y. Cohen, J. Mintorovitch, L. Chileuitt, H. Shimizu, J. Kucharczyk, M. Wendland and P. Weinstein, "Early Detection of Regional Cerebral Ischemia in Cats: Comparison of Diffusion-and T2-weighted MRI and Spectroscopy", *Magnetic Resonance in Medicine*, Vol. 14, No. 2, pp. 330–346, 1990.

11. Warach, S., D. Chien, W. Li, M. Ronthal and R. Edelman, "Fast Magnetic Resonance Diffusion-weighted Imaging of Acute Human Stroke", *Neurology*, Vol. 42, No. 9, pp. 1717–1717, 1992.

12. Gonzalez, R. G., P. W. Schaefer, F. S. Buonanno, L. H. Schwamm, R. F. Budzik, G. Rordorf, B. Wang, A. G. Sorensen and W. J. Koroshetz, "Diffusion-weighted MR Imaging: Diagnostic Accuracy in Patients Imaged within 6 Hours of Stroke Symptom Onset", *Radiology*, Vol. 210, No. 1, pp. 155–162, 1999.

13. Chien, D., K. K. Kwong, D. R. Gress, F. S. Buonanno, R. B. Buxton and B. R. Rosen, "MR Diffusion Imaging of Cerebral Infarction in Humans.", *American Journal of Neuroradiology*, Vol. 13, No. 4, pp. 1097–1102, 1992.

14. Arfanakis, K., V. M. Haughton, J. D. Carew, B. P. Rogers, R. J. Dempsey and M. E. Meyerand, "Diffusion Tensor MR Imaging in Diffuse Axonal Injury", *American Journal of Neuroradiology*, Vol. 23, No. 5, pp. 794–802, 2002.

15. Basser, P. J., J. Mattiello and D. LeBihan, "Estimation of the Effective Self-diffusion Tensor from the NMR Spin Echo", *Journal of Magnetic Resonance, Series*

B, Vol. 103, No. 3, pp. 247–254, 1994.

16. Pierpaoli, C., P. Jezzard, P. J. Basser, A. Barnett and G. Di Chiro, "Diffusion Tensor MR Imaging of the Human Brain.", *Radiology*, Vol. 201, No. 3, pp. 637–648, 1996.

17. Johansen-Berg, H. and T. E. Behrens, *Diffusion MRI: From Quantitative Measurement to in Vivo Neuroanatomy*, Academic Press, 2013.

18. Assaf, Y. and Y. Cohen, "Non-mono-exponential Attenuation of Water and n-acetyl Aspartate Signals Due to Diffusion in Brain Tissue", *Journal of Magnetic Resonance*, Vol. 131, No. 1, pp. 69–85, 1998.

19. Niendorf, T., R. M. Dijkhuizen, D. G. Norris, M. van Lookeren Campagne and K. Nicolay, "Biexponential Diffusion Attenuation in Various States of Brain Tissue: Implications for Diffusion-weighted Imaging", *Magnetic Resonance in Medicine*, Vol. 36, No. 6, pp. 847–857, 1996.

20. Mulkern, R. V., H. Gudbjartsson, C.-F. Westin, H. P. Zengingonul, W. Gartner, C. R. Guttmann, R. L. Robertson, W. Kyriakos, R. Schwartz, D. Holtzman *et al.*, "Multi-component Apparent Diffusion Coefficients in Human Brain^2", *NMR Biomed*, Vol. 12, pp. 51–62, 1999.

21. Mulkern, R. V., S. Vajapeyam, R. L. Robertson, P. A. Caruso, M. J. Rivkin and S. E. Maier, "Biexponential Apparent Diffusion Coefficient Parametrization in Adult vs Newborn Brain", *Magnetic Resonance Imaging*, Vol. 19, No. 5, pp. 659–668, 2001.

22. Einstein, A., "On the Theory of the Brownian Movement", *Annalen Der Physik*, Vol. 4, No. 19, pp. 371–381, 1906.

23. Hahn, E. L., "Spin Echoes", *Physical Review*, Vol. 80, No. 4, p. 580, 1950.

24. Carr, H. Y. and E. M. Purcell, "Effects of Diffusion on Free Precession in Nuclear Magnetic Resonance Experiments", *Physical Review*, Vol. 94, No. 3, p. 630, 1954.

25. Torrey, H. C., "Bloch Equations with Diffusion Terms", *Physical Review*, Vol. 104, No. 3, p. 563, 1956.

26. Stejskal, E. and J. Tanner, "Spin Diffusion Measurements: Spin Echoes in the Presence of A Time-dependent Field Gradient", *The Journal of Chemical Physics*, Vol. 42, No. 1, pp. 288–292, 1965.

27. Callaghan, P. T., *Principles of Nuclear Magnetic Resonance Microscopy*, Oxford University Press, 1993.

28. Latour, L. L., K. Svoboda, P. P. Mitra and C. H. Sotak, "Time-dependent Diffusion of Water in a Biological Model System.", *Proceedings of the National Academy of Sciences*, Vol. 91, No. 4, pp. 1229–1233, 1994.

29. Assaf, Y., D. Ben-Bashat, J. Chapman, S. Peled, I. Biton, M. Kafri, Y. Segev, T. Hendler, A. Korczyn, M. Graif *et al.*, "High b-value Q-space Analyzed Diffusion-weighted MRI: Application to Multiple Sclerosis", *Magnetic Resonance in Medicine*, Vol. 47, No. 1, pp. 115–126, 2002.

30. Stejskal, E., "Use of Spin Echoes in a Pulsed Magnetic-Field Gradient to Study Anisotropic, Restricted Diffusion and Flow", *The Journal of Chemical Physics*, Vol. 43, No. 10, pp. 3597–3603, 1965.

31. Wang, M. C. and G. E. Uhlenbeck, "On the Theory of the Brownian Motion II", *Reviews of Modern Physics*, Vol. 17, No. 2-3, p. 323, 1945.

32. Bloch, F., "Nuclear Induction", *Physical Review*, Vol. 70, No. 7-8, p. 460, 1946.

33. Le Bihan, D., E. Breton, D. Lallemand, P. Grenier, E. Cabanis and M. Laval-Jeantet, "MR Imaging of Intravoxel Incoherent Motions: Application to Diffusion

and Perfusion in Neurologic Disorders.", *Radiology*, Vol. 161, No. 2, pp. 401–407, 1986.

34. Basser, P. J. and C. Pierpaoli, "Microstructural and Physiological Features of Tissues Elucidated by Quantitative-Diffusion-tensor MRI", *Journal of Magnetic Resonance*, Vol. 213, No. 2, pp. 560–570, 2011.

35. Mori, S., B. J. Crain, V. Chacko and P. Van Zijl, "Three-dimensional Tracking of Axonal Projections in the Brain by Magnetic Resonance Imaging", *Annals of Neurology*, Vol. 45, No. 2, pp. 265–269, 1999.

36. Cory, D., "Measurement of Translational Displacement Probabilities by NMR: An Indicator of Compartmentation", *Magnetic Resonance in Medicine*, Vol. 14, No. 3, pp. 435–444, 1990.

37. Callaghan, P. T., "Pulsed-gradient Spin-echo NMR for Planar, Cylindrical, and Spherical Pores Under Conditions of Wall Relaxation", *Journal of Magnetic Resonance, Series A*, Vol. 113, No. 1, pp. 53–59, 1995.

38. Callaghan, P. T., A. Coy, D. MacGowan, K. J. Packer and F. O. Zelaya, "Diffraction-like Effects in NMR Diffusion Studies of Fluids in Porous Solids", , 1991.

39. Tuch, D. S., "Q-ball Imaging", *Magnetic Resonance in Medicine*, Vol. 52, No. 6, pp. 1358–1372, 2004.

40. Özarslan, E., B. C. Vemuri and T. H. Mareci, "Generalized Scalar Measures for Diffusion MRI Using Trace, Variance, and Entropy", *Magnetic Resonance in Medicine*, Vol. 53, No. 4, pp. 866–876, 2005.

41. Cory, D., A. Garroway and J. Miller, "Applications of Spin Transport as A Probe of Local Geometry", *Abstracts of Papers of the American Chemical Society*, Vol. 199, pp. 105–POLY, American Chemical Society 1155 16th st, NW, Washington,

DC 20036, 1990.

42. Mitra, P. P., "Multiple Wave-vector Extensions of the NMR Pulsed-field-gradient Spin-echo Diffusion Measurement", *Physical Review B*, Vol. 51, No. 21, p. 15074, 1995.

43. Özarslan, E., U. Nevo and P. J. Basser, "Anisotropy Induced by Macroscopic Boundaries: Surface-normal Mapping Using Diffusion-weighted Imaging", *Biophysical Journal*, Vol. 94, No. 7, pp. 2809–2818, 2008.

44. Özarslan, E. and P. J. Basser, "Microscopic Anisotropy Revealed by NMR Double Pulsed Field Gradient Experiments with Arbitrary Timing Parameters", *The Journal of Chemical Physics*, Vol. 128, No. 15, p. 154511, 2008.

45. Grebenkov, D. S., "NMR Survey of Reflected Brownian Motion", *Reviews of Modern Physics*, Vol. 79, No. 3, p. 1077, 2007.

46. Grebenkov, D. S., "Analytical Solution for Restricted Diffusion in Circular and Spherical Layers Under Inhomogeneous Magnetic Fields", *The Journal of Chemical Physics*, Vol. 128, No. 13, p. 134702, 2008.

47. Shemesh, N., E. Özarslan, P. J. Basser and Y. Cohen, "Measuring Small Compartmental Dimensions with Low-q Angular Double-PGSE NMR: The Effect of Experimental Parameters on Signal Decay", *Journal of Magnetic Resonance*, Vol. 198, No. 1, pp. 15–23, 2009.

48. Shemesh, N., E. Özarslan, P. J. Basser and Y. Cohen, "Accurate Noninvasive Measurement of Cell Size and Compartment Shape Anisotropy in Yeast Cells Using Double-pulsed Field Gradient MR", *NMR in Biomedicine*, Vol. 25, No. 2, pp. 236–246, 2012.

49. Yolcu, C. and E. Özarslan, "Diffusion-Weighted Magnetic Resonance Signal for General Gradient Waveforms: Multiple Correlation Function Framework, Path

Integrals, and Parallels Between Them", *Visualization and Processing of Higher Order Descriptors for Multi-Valued Data*, p. 3, 2015.

50. Wedeen, V. J., P. Hagmann, W.-Y. I. Tseng, T. G. Reese and R. M. Weisskoff, "Mapping Complex Tissue Architecture with Diffusion Spectrum Magnetic Resonance Imaging", *Magnetic Resonance in Medicine*, Vol. 54, No. 6, pp. 1377–1386, 2005.

51. Özarslan, E., T. M. Shepherd, B. C. Vemuri, S. J. Blackband and T. H. Mareci, "Resolution of Complex Tissue Microarchitecture Using the Diffusion Orientation Transform (DOT)", *NeuroImage*, Vol. 31, No. 3, pp. 1086–1103, 2006.

52. Descoteaux, M., E. Angelino, S. Fitzgibbons and R. Deriche, "Regularized, Fast, and Robust Analytical Q-ball Imaging", *Magnetic Resonance in Medicine*, Vol. 58, No. 3, pp. 497–510, 2007.

53. Aganj, I., C. Lenglet, G. Sapiro, E. Yacoub, K. Ugurbil and N. Harel, "Reconstruction of the Orientation Distribution Function in Single-and Multiple-shell Q-ball Imaging within Constant Solid Angle", *Magnetic Resonance in Medicine*, Vol. 64, No. 2, pp. 554–566, 2010.

54. Özarslan, E., C. G. Koay, T. M. Shepherd, M. E. Komlosh, M. O. İrfanoğlu, C. Pierpaoli and P. J. Basser, "Mean Apparent Propagator (MAP) MRI: A Novel Diffusion Imaging Method for Mapping Tissue Microstructure", *NeuroImage*, Vol. 78, pp. 16–32, 2013.

55. Ozarslan, E., M. Avram, P. Basser and C.-F. Westin, "Rotating Field Gradient (RFG) MR for Direct Measurement of the Diffusion Orientation Distribution Function (dODF)", *in ISMRM Scientific Workshop on Diffusion as a Probe of Neural Tissue Microstructure, Podstrana, Croatia, 2013.*.

56. Avram, M., J. Sarlls, P. Basser and E. Ozarslan, "Rotating Field Gradient (RFG) Diffusion MRI for Mapping 3D Orientation Distribution Functions (ODFs) in the

Human Brain", *The International Society for Magnetic Resonance in Medicine, 2014, vol. 22, p. 4453.*.

57. Özarslan, E., M. Memic, A. Avram, M. Afzali, P. Basser and C.-F. Westin, "Rotating Field Gradient (RFG) MR Offers Improved Orientational Sensitivity", *Biomedical Imaging (ISBI), 2015 IEEE 12th International Symposium on*, pp. 955–958, IEEE, 2015.

58. Özarslan, E., C. G. Koay and P. J. Basser, "Simple Harmonic Oscillator Based Reconstruction and Estimation for One-dimensional Q-space Magnetic Resonance (1D-SHORE)", *Excursions in Harmonic Analysis, Volume 2*, pp. 373–399, Springer, 2013.